iScience

CellPress
OPEN ACCESS

Article

Akkermansia muciniphila induces mitochondrial calcium overload and α -synuclein aggregation in an enteroendocrine cell line

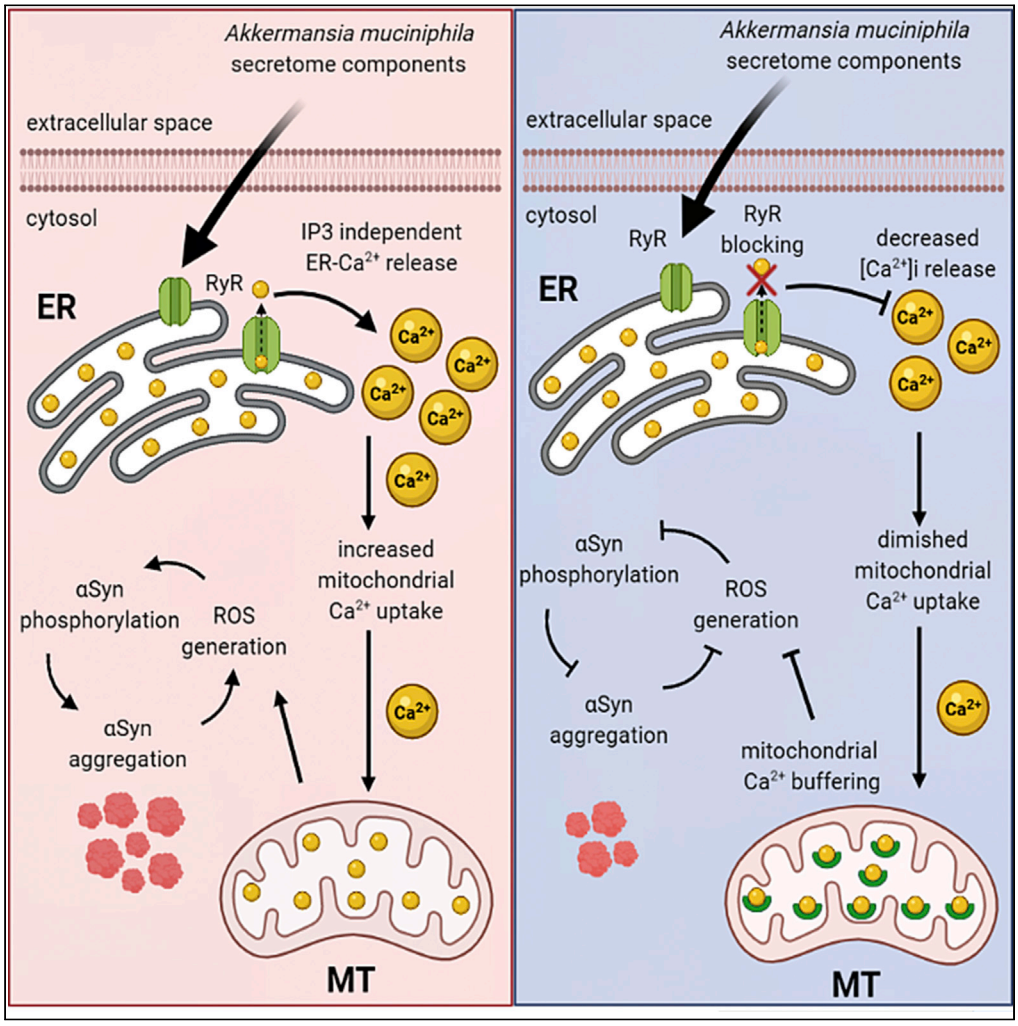

Dionísio Pedro Amorim Neto, Beatriz Pelegrini Bosque, João Vitor Pereira de Godoy, ..., Hernandes Faustino de Carvalho, Christian González-Billault, Matheus de Castro Fonseca

matheus.fonseca@lnbio.cnpem.br

Highlights

Gut bacterium *Akkermansia muciniphila* is increased in patients with Parkinson disease

A. muciniphila-conditioned medium induces mitochondrial Ca^{2+} overload in EECs

Mitochondrial Ca^{2+} overload leads to ROS generation and αSyn aggregation *in vitro*

Buffering mitochondrial Ca^{2+} inhibits *A. muciniphila*-induced αSyn aggregation

Amorim Neto et al., iScience *25*, 103908
March 18, 2022
https://doi.org/10.1016/j.isci.2022.103908

iScience

CellPress
OPEN ACCESS

Article

Akkermansia muciniphila induces mitochondrial calcium overload and α -synuclein aggregation in an enteroendocrine cell line

Dionísio Pedro Amorim Neto,[1,2] Beatriz Pelegrini Bosque,[1,2] João Vitor Pereira de Godoy,[1,2] Paulla Vieira Rodrigues,[1,2] Dario Donoso Meneses,[1] Katiane Tostes,[1] Celisa Caldana Costa Tonoli,[1] Hernandes Faustino de Carvalho,[2] Christian González-Billault,[3,4,5,6] and Matheus de Castro Fonseca[1,2,7,*]

SUMMARY

The gut microbiota influence neurodevelopment, modulate behavior, and contribute to neurodegenerative disorders. Several studies have consistently reported a greater abundance of *Akkermansia muciniphila* in Parkinson disease (PD) fecal samples. Therefore, we investigated whether *A.muciniphila*-conditioned medium (CM) could initiate α-synuclein (αSyn) misfolding in enteroendocrine cells (EEC) — a component of the gut epithelium featuring neuron-like properties. We found that *A. muciniphila* CM composition is influenced by the ability of the strain to degrade mucin. Our *in vitro* experiments showed that the protein-enriched fraction of mucin-free CM induces RyR-mediated Ca^{2+} release and increased mitochondrial Ca^{2+} uptake leading to ROS generation and αSyn aggregation. Oral administration of *A. muciniphila* cultivated in the absence of mucin to mice led to αSyn aggregation in cholecystokinin (CCK)-positive EECs but no motor deficits were observed. Noteworthy, buffering mitochondrial Ca^{2+} reverted the damaging effects observed. These molecular insights offer evidence that bacterial proteins can induce αSyn aggregation in EECs.

INTRODUCTION

Traditionally, Parkinson disease (PD) has been characterized as a progressive neurodegenerative disorder caused by loss of dopaminergic neurons in the *substantia nigra pars compacta* of the midbrain (Davie, 2008). Neuronal loss leads to Parkinsonism, an array of motor symptoms comprehending muscle rigidity, slowness, tremors, and difficulty in controlling movement (Bernheimer et al., 1973). However, recent studies have shown that drug-naive patients with PD frequently report gastrointestinal complaints such as constipation, nausea, and prolonged intestinal transit time even years before the disease is diagnosed (Adams-Carr et al., 2016; Martinez-Martin et al., 2011; Mun et al., 2016). Therefore, this pathology is now considered as a multisystemic disease, gathering a plethora of non-motor symptoms (Chaudhuri et al., 2006; Greenland et al., 2019).

Currently, PD is the second most common neurodegenerative disease and the interest of the scientific community to unveil the cellular and molecular mechanisms of this complex pathology has grown substantially, triggered especially by the discovery of a number of causative monogenic mutations (Bekris et al., 2010). Nevertheless, these mutations only explain a small percentage of all PD cases since about 90% are sporadic (de Lau and Breteler, 2006).

The key dogma of PD consists in the aggregation of the protein alpha-synuclein (αSyn) within neurons (Spillantini et al., 1997). This presynaptic protein is linked genetically and neuropathologically to PD. It is accepted that αSyn aberrant soluble oligomeric conformations (protofibrils) are the toxic species that disrupt cellular homeostasis and lead to neuronal death through effects on several intracellular targets, including synaptic function (Stefanis, 2012). This aggregation process can be caused by genetic or sporadic factors due to mitochondrial dysfunction, oxidative stress, and altered proteostasis (Greenamyre and Hastings, 2004). Although this toxic aggregation occurs more widely throughout the central system, abundant clinical and pathological evidence shows that misfolded αSyn is found in enteric nerves before it appears in

[1]Brazilian Biosciences National Laboratory (LNBio), Brazilian Center for Research in Energy and Materials (CNPEM), 10000 Giuseppe Maximo Scolfaro St., 13083-100 Campinas, São Paulo, Brazil

[2]Department of Structural and Functional Biology, State University of Campinas, Campinas, São Paulo, Brazil

[3]Department of Biology, Faculty of Sciences and Department of Neurosciences, Faculty of Medicine, Universidad de Chile, Santiago, Chile

[4]Department of Neurosciences, Faculty of Medicine, Universidad de Chile, Santiago, Chile

[5]Geroscience Center for Brain Health and Metabolism, Santiago, Chile

[6]The Buck Institute for Research on Aging, Novato, CA 94945, USA

[7]Lead contact

*Correspondence: matheus.fonseca@lnbio.cnpem.br

https://doi.org/10.1016/j.isci.2022.103908

the brain (Braak and Del Tredici, 2009; Braak et al., 2003a; Hawkes et al., 2010). It was recently reported that enteroendocrine cells (EECs), which are part of the gut epithelium and are directly exposed to the gut lumen and its microbiome, possess many neuron-like properties, such as αSyn expression, and connect to enteric nerves (Chandra et al., 2017). This leads to the hypothesis that PD might originate in the gut and then spread to the CNS via cell-to-cell prion-like propagation (Chandra et al., 2017). Such a concept has gathered significant momentum in recent years and great attention has been given to the brain-gut connection. Therefore, the gut microbiome raises as a promising target to be investigated in the outcome of sporadic PD. Several reports have shown that individuals with PD display an imbalanced gut microbiome (dysbiosis) (Heintz-Buschart et al., 2018; Hill-Burns et al., 2017; Keshavarzian et al., 2015) where commensal bacteria (e.g., phylum Firmicutes) are reduced, while pathogenic Gram-negative bacteria (*Proteobacteria* sp, Enterobacteriaceae sp, *Escherichia* sp.) and mucin-degrading Verrucomicrobiaceae, such as *A. muciniphila*, are increased (Hill-Burns et al., 2017; Keshavarzian et al., 2015; Li et al., 2017; Scheperjans et al., 2015; Unger et al., 2016).

The mucin-degrading microorganism *A. muciniphila* (Derrien et al., 2004) comprises about 1%–4% of the fecal microbiome in humans (Naito et al., 2018). While numerous diseases have been associated with a decrease in *A. muciniphila* abundance (Grander et al., 2018; Schneeberger et al., 2015), an increase of this microorganism has been consistently reported in patients with PD (Baldini et al., 2020). In addition, it was shown that *A. muciniphila* abundance had the largest contribution to the significantly altered metabolite secretion profiles of patients with sporadic PD (Baldini et al., 2020).

The microbial surface and secreted proteins contain many proteins that interact with other microbes, host, and/or environment (Tjalsma et al., 2000). These proteins (e.g., receptors, transporters, adhesins, secreted enzymes, and toxins) not only allow bacteria to interact with and adapt to their environment but also modulate the host cells activities (Gagic et al., 2016). Identifying the effects of *A. muciniphila* metabolites and/or secreted proteins on the physiology of EECs could therefore increase our current understanding on the cell mechanisms that could lead to one of the possible outcomes of sporadic PD.

Based on the common occurrence of gastrointestinal symptoms in PD, dysbiosis among patients with PD, and strong evidence that the microbiota influences CNS function, in this work we investigated whether and how *A. muciniphila* CM alters EECs homeostasis leading to αSyn aggregation. Herein, we found that the *A. muciniphila* CM composition depends on whether mucin is present during culture and is correlated with the ability of the strain to degrade and utilize mucin. In addition, we observed that, *in vitro,* only the thermo-sensitive protein-enriched fraction of mucin-free CM induces inositol 1,4,5-trisphosphate (IP_3)-independent ER(ER)-calcium (Ca^{2+}) release by modulating ryanodine receptors (RyR), leading to increased αSyn expression and mitochondrial Ca^{2+} uptake. RyR-mediated mitochondrial Ca^{2+} overload led to ROS generation culminating with αSyn aggregation. Noteworthy, blocking RyR decreased mitochondrial Ca^{2+} overload and αSyn phosphorylation. Moreover, buffering mitochondrial Ca^{2+} strongly prevented αSyn aggregation in EECs *in vitro*. On the other hand, none of the strategies could diminish CM-induced αSyn overexpression mediated by GATA-2 suggesting this mechanism to be independent on RyR-dependent Ca^{2+} signaling. *In vivo* experiments showed that increasing the levels of *A. muciniphila* by oral administration in aged mice was not sufficient to cause any motor deficits, however, increased αSyn aggregation in EECs. Therefore, the molecular insights provided here motivate future studies to address functional changes in neurologic phenotypes that might be correlated with of *A. muciniphila* levels in the gut.

RESULTS

A. muciniphila growth curve pattern and conditioned medium composition are modulated by mucin

A. muciniphila is a mucin-degrading Gram-negative bacterium of the phylum Verrucomicrobia (Derrien et al., 2004). However, the intestinal mucus layer is thought to be inversely correlated with *A. muciniphila* abundance in the gut (Sovran et al., 2019). Prolonged lack of dietary fibers induces damage to the mucus barrier and is directly associated with increased abundance of *A. muciniphila*. This would bring gut bacteria closer to the intestinal epithelium, which could trigger deleterious effects or other host compensatory responses (Desai et al., 2016). To test whether mucin could interfere with *A. muciniphila* CM composition, the strain DSM-22959 was harvested and monitored for 72 h in both BHI culture medium and BHI supplemented with 0.4% mucin (from porcine stomach, Type II) (Figure 1A).

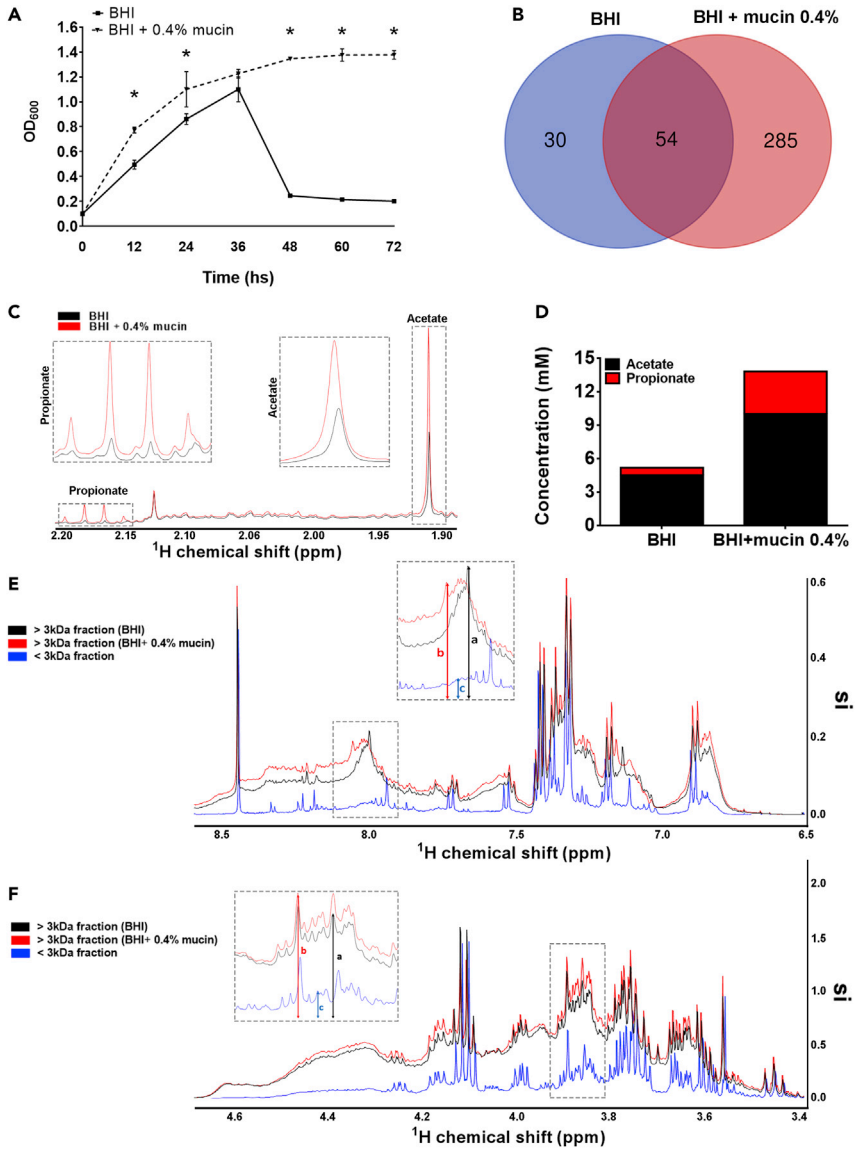

Figure 1. Growth curve of *A. muciniphila* and conditioned media characterization

(A) Growth curve as a function of culture media supplementation. (Error bars indicate the media ±SEM of six individual bacterial culture for each condition; unpaired *Student'l's t-test*, *p < 0.05).

(B) Qualitative Venn diagram showing the common and unique expressed proteins between the 0.4% mucin and mucin-free culture condition identified by mass spectrometry. Mass spectrometry data were obtained from at least six vials for each culture condition.

(C) Representative 500 MHz ^{1}H NMR spectra of *A. muciniphila* conditioned BHI (black line) and BHI+0.4% mucin (red line) with acetate and propionate labeled. Inserts show zoom of the metabolites spectra.

(D) Graph represents ^{1}H NMR quantification of acetate (black) and propionate (red) concentration in both conditioned media (BHI: acetate – 4.52mM ± 0.01mM; propionate: 0.67 ± 0.03mM. BHI + mucin 0.4%: acetate – 10.02 ± 0.18mM; propionate: 3.8–0.2mM).

(E) and (F) shows a comparison of protein content evaluated by 500 MHz 1H NMR spectra of > 3kDa fraction of *A. muciniphila* conditioned BHI (black line) and BHI+0.4% mucin (red line) and < 3kDa fraction (flow-through) of BHI CM (blue line). Protein side-chain H^{N} is shown in (E) and H^{α} is shown in (F). Inserts highlight representative peaks in the chemical shift portraying enlarged profile (A and B) in > 3kDa fractions when compared to <3kDa fraction (C). See also Figure 1B and Table S1.

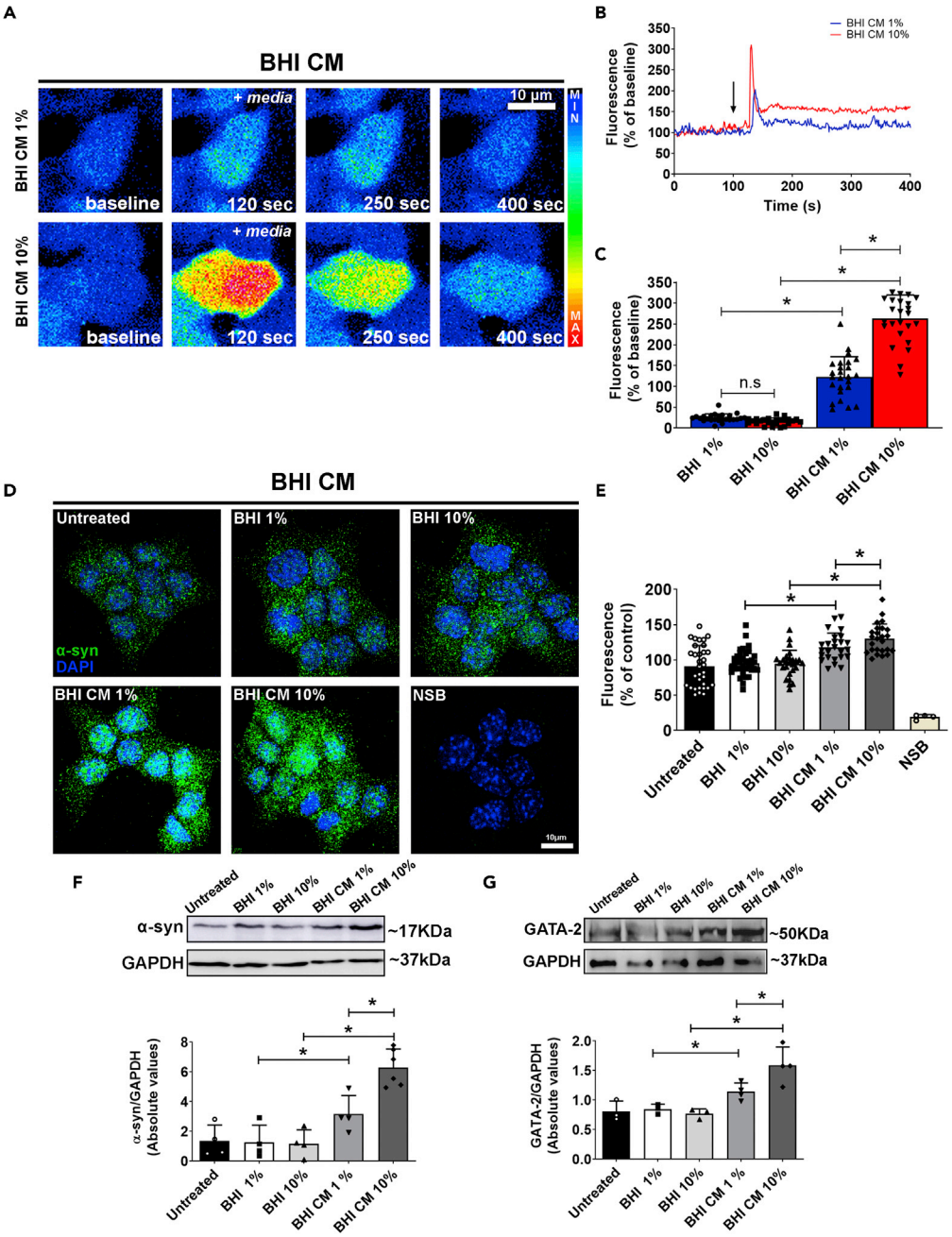

Figure 2. *Akkermansia muciniphila* conditioned medium induces intracellular calcium signals and increased levels of α-synuclein in STC-1 cells

(A) Confocal microscopy imaging of STC-1 cells incubated with Fluo-4/AM (6μM) and stimulated with 1% or 10% >3kDa fraction of mucin-free *A. muciniphila* conditioned medium (BHI CM) (scale bar: 10 μm).

(B) Representative time-course of total Ca^{2+} signal. Arrow indicates the moment when culture medium was applied.

(C) Quantification of the peak fluorescence following stimulation with 1% or 10% conditioned (BHI CM) and unconditioned (BHI) media. (Error bars indicate the media ±SEM; n = at least 25 cells for each group, *p < 0.05 by unpaired Student's *t-test*).

(D) αSyn staining (green) in STC-1 cells after 48-h incubation with 1%–10% conditioned (BHI CM) or unconditioned media (BHI) demonstrating increased expression of the protein. Nuclei were stained with DAPI (blue) and immunofluorescence control is shown as NSB (non-specific binding control) (scale bar: 10 μm).

(E) Quantification of αSyn fluorescence intensity in images shown in (D). (Data are represented as mean ± SEM; n = at least 25 cells for each group from three individual experiments, *p < 0.05 by unpaired Student's *t-test*).

Figure 2. *Continued*

(F) Immunoblots (upper image) of total cell lysates showing the increased expression of αSyn after 48-hincubation with 1%–10% conditioned (BHI CM) or unconditioned medium (BHI). Densitometric analysis shows increased expression of αSyn in 1%–10% BHI CM condition when compared to 1%–10% BHI. (Data are represented as mean ± SEM; n = 4 individual experiments, *p < 0.05 by two-way Student's *t-test*).

(G) Immunoblots (upper image) of total cell lysates showing the increased expression of GATA-2 after 48-hincubation with 1%–10% conditioned (BHI CM) or unconditioned media (BHI). Densitometric analysis shows increased expression of GATA-2 in 1%–10% BHI CM condition when compared to 1%–10% BHI. (Data are represented as mean ± SEM; n = 3 individual experiments; *p < 0.05 by unpaired Student's *t-test*). See also Figure Figures S1–S6.

It is clearly observed that the addition of mucin maintains the growth of *A. muciniphila* in BHI medium (Figure 1A). When mucin was provided, *A. muciniphila* grew faster at log phase and maintained a plateau for a longer time than when cultivated in mucin-free BHI medium. In addition, when analyzing the protein-enriched fraction of the CM (fraction with proteins >3kDa), separated from the metabolite-enriched fraction (flow-through) under fractioning with 3kDa filters, we identified 285 differentially expressed proteins in the CM obtained from *A. muciniphila* cultivated for 36–40 h (peak of growth for both conditions) in 0.4% mucin-supplemented BHI medium as opposed to 30 in mucin-free medium (Figure 1B and Table S1). In both cases, many of these proteins have not yet been characterized by the scientific community. Therefore, *A. muciniphila* CM composition is dependent on the presence of mucin during culture.

To confirm whether mucin added to the culture media is effectively metabolized by *A. muciniphila*, we evaluated acetate and propionate levels of the complete mucin-free and mucin-supplemented media by Nuclear Magnetic Resonance (NMR). We detected a ∼2.2- and a ∼5.6-fold increase in acetate and propionate levels in mucin-supplemented CM, respectively, when compared to mucin-free medium (Figures 1C and 1D). In addition, ^{1}H NMR analysis also confirmed that after passing through 3kDa cut-off membrane, the flow-through fraction of the CM was enriched in small molecules and bacterial metabolites (<3kDa fraction) while the broader spectrum exhibited by the non-filtered fraction along the chemical shift profiled a sample mostly composed of >3kDa proteins (>3kDa fraction) (Figures 1E and 1F).

Intracellular calcium signaling is elicited by *A. muciniphila* mucin-free conditioned medium in a model of enteroendocrine cells

Enteroendocrine cells (EECs) are chemosensory cells distributed throughout all the mucosal lining of the intestine and with their apical surface exposed to the lumen of the organ. In addition, it was recently described that EECs also connect to enteric neurons (Bohorquez et al., 2015; Chandra et al., 2017; Liddle, 2018). Owing to their location at the interface between gut contents and the nervous system, EECs provide a direct route for substances in the gut to affect neural function. The STC-1 cell line is widely accepted as a model of native EECs (McCarthy et al., 2015) due to the expression of several gastrointestinal hormones, including cholecystokinin (CCK) and peptide YY (PYY), whose secretion pattern is compared to that of native EECs (Hand et al., 2012, 2013; Wang et al., 2002). In addition, these cells present many neuronal-like features, including the expression of αSyn (Chandra et al., 2017). Because native EECs are hard to culture or to be collected from intestinal tissue in a sufficient number for *in vitro* assays, STC-1 is considered an attractive cell model for evaluating properties of EECs.

Calcium (Ca^{2+}) is known to regulate several important cell functions, such as secretion, proliferation, apoptosis, protein biosynthesis, and folding (Alvarenga et al., 2016; Fonseca et al., 2018; Guimaraes et al., 2017). In order to study the effects of *A. muciniphila* CM in the fluctuations of intracellular Ca^{2+} signaling in STC-1 cells, we first stimulated Fluo-4/AM-loaded cells with 1% or 10% conditioned BHI medium (BHI CM) or unconditioned BHI medium (BHI). We observed that *A. muciniphila* mucin-free BHI CM induces a strong increase in Ca^{2+} transient in a concentration-dependent manner (Figures 2A–2C). On the other hand, 0.4% mucin-supplemented BHI CM induced weaker Ca^{2+} signals when compared to the mucin-free condition (Figure 2 and S1A–S1C). In order to observe whether this Ca^{2+} fluctuation was due to bacterial secreted elements and not to the unconditioned culture medium, STC-1 cells were also stimulated with mucin-supplemented and mucin-free unconditioned media (BHI) and no fluctuation on intracellular Ca^{2+} signals was observed (Figure S2).

Therefore, > 3kDa secreted elements found in *A.muciniphila* CM are key to elicit intracellular Ca^{2+} response in STC-1 cells.

Mucin-free *A. muciniphila* conditioned medium increases expression of endogenous α-synuclein in STC-1 cells

Induced transient increase in free intracellular Ca^{2+} concentration by thapsigargin or Ca^{2+} ionophore chemical treatments lead to a significant increase in the number of cells presenting microscopically visible αSyn aggregates (Nath et al., 2011). Also, it is already reported that increased expression or decreased degradation of αSyn can initiate the formation of amyloid aggregates that can assemble to form Lewy bodies and Lewy neurites over the course of a lifetime (Hijaz and Volpicelli-Daley, 2020).

In addition, misfolded αSyn is found in enteric nerves before it appears in the brain (Braak and Del Tredici, 2009; Braak et al., 2003a; Hawkes et al., 2010). However, it is yet to be demonstrated whether the secreted proteins of a gut bacterium could initiate this pathologic sequence of events.

Therefore, we next analyzed whether *A. muciniphila* CM could modulate αSyn homeostasis in STC-1 cells. MTS assay confirmed that 48-h incubation of cells with 1% or 10% BHI CM or BHI did not decrease cell viability (Figure S3). When STC-1 cells were incubated with 1% or 10% mucin-free BHI CM for 48 h, but not with the unconditioned one (BHI), we detected a significant clear overexpression of αSyn analyzed by immunofluorescence and Western blotting (Figures 2D–2F). However, this was not observed when the cells were incubated with 0.4% mucin-containing BHI CM (Figures S1D–S1F).

The SNCA gene expression in neurons, which encodes for αSyn, is known to be controlled by the GATA-2 transcription factor (Scherzer et al., 2008), which also plays a crucial role in CNS development, and erythroid cells differentiation (Nardelli et al., 1999). In addition, GATA-2 has a critical role in neuronal development, particularly in cell fate specification of catecholaminergic sympathetic neurons (Bilodeau et al., 2001; Tsarovina et al., 2004). We observed that STC-1 cells not only express GATA-2 transcription factor but also exhibit increased expression of this factor when incubated with either 1% or 10% mucin-free *A. muciniphila* BHI CM. This supports the idea that *A.muciniphila* conditioned medium upregulates GATA-2 which in turn induces SNCA overexpression (Figure 2G).

To explore deeper the effects of *A. muciniphila* mucin-free CM and to understand whether these phenomena were specifically due to the protein-enriched fraction of *A. muciniphila* CM, we stimulated STC-1 cells with 1% and 10% of heat-inactivated BHI CM and observed no fluctuation on Ca^{2+} signaling neither alteration on αSyn homeostasis evaluated by western blotting for GATA-2, αSyn, and pser-129 αSyn (Figure S4). In addition, to rule out possible effects of the metabolite-enriched fraction of *A. muciniphila* CM (<3kDa fraction), we performed the same set of experiments using this fraction as stimulus and no significant effects on the parameters mentioned above were detected (Figure S5).

Next, we conducted the same set of above experiments employing *Escherichia coli* (*E. coli*) CM to confirm if these observed effects were specifically due to *A. muciniphila* CM. *E. coli* was chosen because it is an abundant Gram-negative microorganism from the gut. This strain was also cultivated in BHI medium under anaerobic condition as for *A. muciniphila* and CM was filtered through 3kDa cut-off membranes. Although we also observed a transient increase in free intracellular Ca^{2+} in STC-1 cells stimulated with 1% or 10% *E. coli* BHI CM (>3kDa fraction), the amplitude of the signal was smaller than the one elicited by *A. muciniphila* (Figures S6A–S6E). In addition, we did not detect alteration on αSyn expression levels when STC-1 cells were incubated for 48 h with *E. coli* CM (Figures S6F–S6H). Ca^{2+} oscillations are ubiquitous signals present in all cells and work as efficient means to transmit intracellular information. The specific oscillatory pattern of response upon binding on ligands to membrane receptors or spontaneously is codified by downstream effectors that subsequently activate different cellular processes. This signal transduction can occur through frequency modulation or amplitude modulation (Smedler and Uhlen, 2014; Tompa et al., 2001). For example, it was recently demonstrated that the oscillation amplitude, not the frequency of cytosolic Ca^{2+}, regulates apoptosis induction (Qi et al., 2020). Although *E.coli* CM Ca^{2+} oscillation pattern with frequency similar to *A. muciniphila* CM, the amplitude of the signal was reduced. These differences seem to be critical when it comes from αSyn homeostasis because *E. coli* CM did not disturb αSyn expression.

In summary, the heat-sensitive protein-enriched fraction of *A. muciniphila* mucin-free CM leads to a transient increase in free intracellular Ca^{2+} and induces GATA2-regulated-overexpression of αSyn in the STC-1 enteroendocrine cell model *in vitro*.

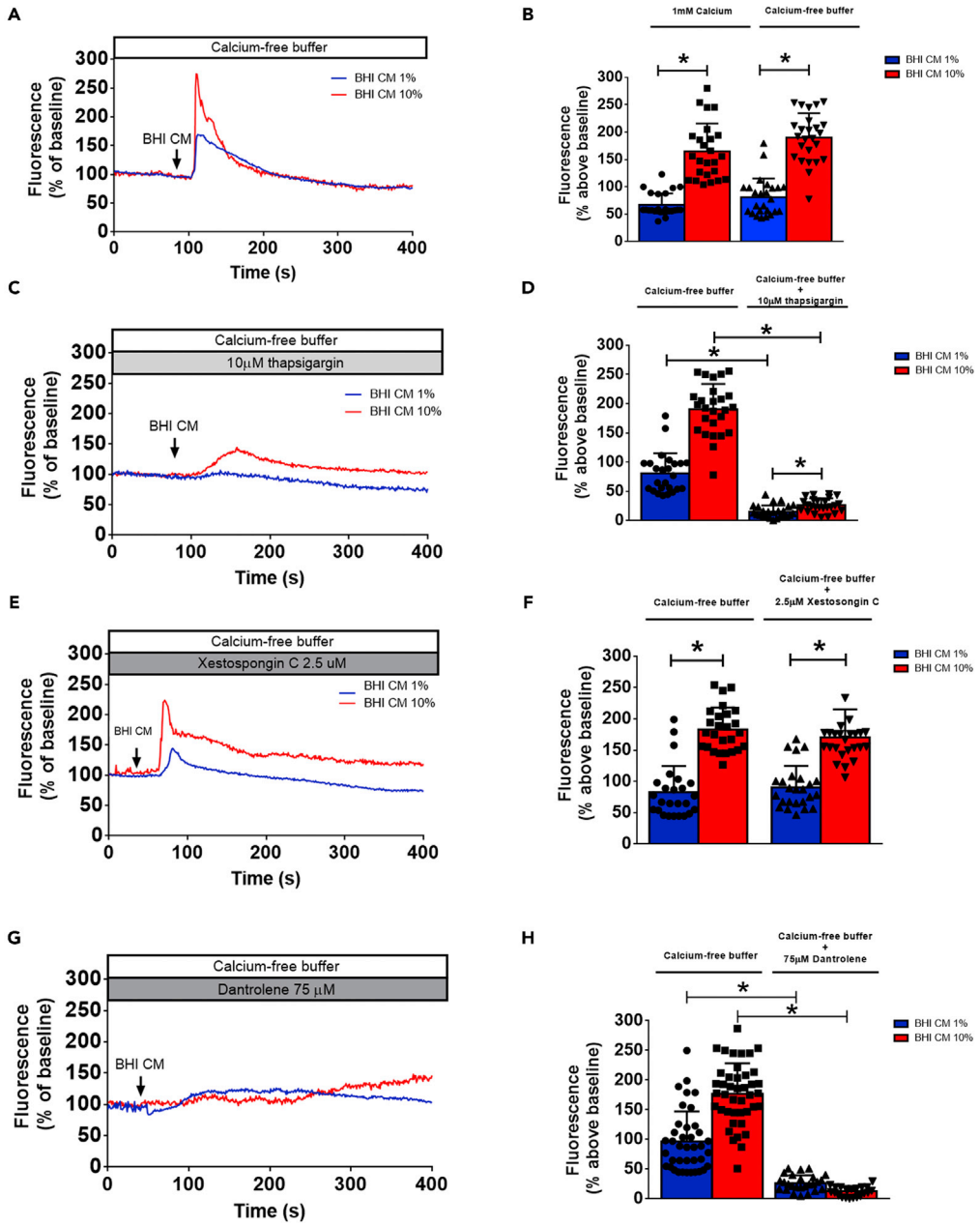

Figure 3. *Akkermansia muciniphila* conditioned medium induces InsP3-independent intracellular calcium signals by acting directly on ryanodine receptors

(A) STC-1 cells were stimulated with 1% or 10% *A. muciniphila* conditioned media (BHI CM) in the presence of Ca^{2+}-free buffer. Graph shows a representative time-course of total Ca^{2+} signal in STC-1cells. The arrow indicates the time when culture medium was applied.

(B) Quantification of the peak fluorescence following cells stimulation with 1% or 10% conditioned (BHI CM) and unconditioned (BHI) media in the presence of 1 mM Ca^{2+} buffer or Ca^{2+}-free buffer.

(C) STC-1 cells were incubated with 10 μM thapsigargin for 30 min and stimulated with 1% or 10% *A. muciniphila* conditioned media (BHI CM) in the presence of Ca^{2+}-free buffer containing 10 μM thapsigargin. Graph shows a representative time-course of total Ca^{2+} signal in STC-1 cells. Arrow indicates the time when culture medium was applied.

(D) Quantification of the peak fluorescence following cells stimulation with 1% or 10% conditioned (BHI CM) and unconditioned (BHI) media shows that the Ca^{2+} signal induced by BHI CM is blocked by 10 μM thapsigargin.

(E) STC-1 cells were incubated with 2.5 μM xestospongin C for 30 min and stimulated with 1% or 10% *A. muciniphila* conditioned media (BHI CM) in the presence of Ca^{2+}-free buffer containing 2.5 μM xestospongin (C) Graph shows a

Figure 3. *Continued*
representative time-course of total Ca^{2+} signal in STC-1 cells. The arrow indicates the time when culture medium was applied.
(F) Quantification of the peak fluorescence following cells stimulation with 1% or 10% conditioned (BHI CM) and unconditioned (BHI) media shows that the Ca^{2+} signal induced by BHI CM is not blocked by the InsP3 receptor inhibitor xestospongin C (2.5 μM).
(G) STC-1 cells were incubated with 75 μM dantrolene for 30 min and stimulated with 1% or 10% *A. muciniphila* conditioned media (BHI CM) in the presence of Ca^{2+}-free buffer containing 75μM dantrolene. Graph shows a representative time-course of total Ca^{2+} signal in STC-1cells. The arrow indicates the time when culture medium was applied.
(H) Quantification of the peak fluorescence following cells stimulation with 1% or 10% conditioned (BHI CM) and unconditioned (BHI) media shows that the Ca^{2+} signal induced by BHI CM is completely blocked by the RyR receptor inhibitor, dantrolene (75 μM). Data in (A), (C), (E), and (G) represent a representative tracing recorded from one individual STC-1 cell of each group. Data in (B), (D), (F), and (H) represented as mean ± SEM of three independent experiments in which at least 25 individual cells were analyzed for calcium transient. *$p < 0.05$ by one-way Student's *t-test*). See also Figure S7.

A. muciniphila conditioned medium induces calcium release from stores in the ER in an IP_3-independent manner

Because we only observed significant effects in αSyn homeostasis in STC-1 cells when working with >3kDa fraction of *A. muciniphila* mucin-free CM, the next set of experiments were performed with this fraction. Several maneuvers were performed to define the mechanism by which *A. muciniphila* mucin-free CM increases free cytoplasmic Ca^{2+} in STC-1 cells. To determine the source of the Ca^{2+}, cells were stimulated in Ca^{2+}-free medium. We observed that *A.muciniphila* CM induced cytoplasmic Ca^{2+} oscillations in a concentration-dependent manner even in Ca^{2+}-free medium (Figures 3A and 3B). Additionally, induced Ca^{2+} signals initiate/predominate in the cytoplasm (Figure S7) and were elicited in a similar fraction of STC-1 cells regardless of the presence of extracellular Ca^{2+}. On the other hand, selective depletion of stored calcium by 10μM thapsigargin significantly blocked Ca^{2+} oscillations induced by *A. muciniphila* CM (Figures 3C and 3D). Thereby, these findings demonstrate that *A. muciniphila* CM sample increases cytoplasmic Ca^{2+} levels by mobilizing intracellular Ca^{2+} stores.

A classic manner by which extracellular factors initiate an intracellular Ca^{2+} mobilization is by generating InsP3 to bind and release Ca^{2+} from InsP3 receptors in the ER (Divecha et al., 1991). In order to investigate whether the cytoplasmic Ca^{2+} increase was triggered by InsP3 generation, we stimulated STC-1 cells in the presence of the InsP3 receptor inhibitor xestospongin C (Gafni et al., 1997). Incubation of cells for 30 min and continuous perfusion with 2.5 μM xestospongin C did not impair *A. muciniphila* CM-induced Ca^{2+} mobilization, suggesting an InsP3-independent release of intracellular Ca^{2+} stores (Figures 3E and 3F). To explore the mechanism by how *A. muciniphila* CM evokes Ca^{2+} release from intracellular stores, we incubated cells for 30 min with dantrolene (75 μM), an inhibitor of Ca^{2+} release through ryanodine receptor (RyR) channels (Hainaut and Desmedt, 1974; Morgan and Bryant, 1977; Zhao et al., 2001). In the presence of 75 μM dantrolene, only a very small Ca^{2+} increase was observed following stimulation with 1% or 10% of *A. muciniphila* CM (Figures 3G and 3H).

Thus, dantrolene strongly abolished *A. muciniphila* CM-induced Ca^{2+} response in EECs *in vitro*. Taken together, these results show that proteins contained in *A. muciniphila* CM work as a physiological RyR-gating agent, eliciting intracellular Ca^{2+} signals by directly modulating RyR.

Mitochondrial calcium overload and impaired membrane potential (ΔΨm) is elicited by *A. muciniphila* conditioned medium

Global changes in Ca^{2+} homeostasis accompanied by the alteration in cellular bioenergetics status and thereby imposing oxidative stress in cells are reported in PD (Ludtmann and Abramov, 2018; Surmeier and Schumacker, 2013). The cytosolic Ca^{2+} concentration in unstimulated cells is maintained at low levels (~100 nM) by several enzymes that translocate Ca^{2+} ions into intracellular stores or across the plasma membrane. Moreover, Ca^{2+} uptake into the mitochondria is not only limited to the control of organelle function but also has a direct impact on the intracellular Ca^{2+} signals evoked by agonist stimulation in the cytosol through modulation of their kinetics and spatial dimensions (Tinel et al., 1999). Enhanced cytosolic Ca^{2+} concentration, on the other hand, affects the bioenergetics of the cells by promoting increased ATP demand (Hill et al., 2012). Furthermore, this alteration in cytosolic Ca^{2+} hampers the normal Ca^{2+} handling by various intracellular organelles, including mitochondria, and threatens neuronal

survival. Although well established for neuronal cells, there is still a gap regarding changes in mitochondrial Ca^{2+} dynamics in EECs due to gut microbiome stimulation and how this event might be related to αSyn homeostasis.

Thereby, we aimed at evaluating mitochondrial Ca^{2+} under stimulation with *A. muciniphila* CM. When STC-1 cells loaded with the mitochondrial Ca^{2+} indicator Rhod-2/AM dye were stimulated with 10% of *A. muciniphila* CM, we observed a significant increase in mitochondrial Ca^{2+} uptake when compared to unconditioned BHI medium (Figures 4A and 4B). In addition, when we incubated the cells for 48 h with 1% or 10% CM and stimulated with ATP (10 μM), mitochondrial fluorescence was dramatically increased in the group incubated with 10% BHI CM when compared to 1% BHI CM or unconditioned BHI medium (1% and 10%) suggesting that long exposure to *A. muciniphila* CM induces increased uptake of Ca^{2+} by the mitochondria (Figures 4C and 4D).

As previously mentioned, enhanced, or sustained Ca^{2+} stress results in mitochondrial injury due to Ca^{2+} overload. Excessive mitochondrial Ca^{2+} uptake or impaired Ca^{2+} efflux influences mitochondrial membrane potential ($\Delta\Psi m$) leading to depolarization of mitochondrial inner membrane, swelling of the organelle, and ultimately cell death (Calvo-Rodriguez et al., 2020; Di Lisa and Bernardi, 2009; Williams et al., 2013). In order to observe whether mitochondrial Ca^{2+} uptake induced by *A. muciniphila* CM could lead to mitochondrial damage, we monitored $\Delta\Psi m$ in STC-1 cells under *A. muciniphila* CM incubation for 48 h. After treatment, cells were stained with the mitochondrial-targeted probe Mitotracker Red CMXRos, which accumulates in mitochondria depending on its membrane potential and has been widely used as an indicator of reduced $\Delta\Psi m$ (Jacotot et al., 2000a, 2000b). As can be observed on Figures 4E and 4F, cells incubated with 10% CM presented a reduced fluorescent signal of the probe which suggests impaired membrane potential.

To identify whether mitochondrial Ca^{2+} overload induced by *A. muciniphila* CM is directly modulated by RyR activation, we repeated the mitochondrial Ca^{2+} assays now in the presence of 75μM dantrolene. As shown in Figures S8A and S8B, BHI CM elicited a strong increase in mitochondrial Ca^{2+}, but this was efficiently reduced in cells previously incubated with dantrolene (Figures S8A and S8B). Altogether, the results described so far demonstrate that *A. muciniphila* mucin-free CM induces exacerbated mitochondrial Ca^{2+} uptake due to misbalanced RyR-mediated intracellular Ca^{2+} signaling, which in turn is the driven force that causes mitochondrial damage, reflected by a loss of membrane $\Delta\Psi m$.

Increased intracellular ROS level, α-synuclein phosphorylation, and aggregation as a consequent event of *A. muciniphila* conditioned medium stimulation of enteroendocrine cells

It is suggested that endogenous ROS mainly modulate cell signaling locally and stimuli that promote ROS formation or mitochondrial alterations highly correlate with mutant αSyn phosphorylation at serine 129 (Ser129), a promoter of αSyn aggregation propensity and toxicity in PD (Karampetsou et al., 2017; Perfeito et al., 2014; Tenreiro et al., 2014). Therefore, we next measured intracellular levels of ROS under stimulation with 1% or 10% *A. muciniphila* CM by live cell imaging. STC-1 cells were incubated for 30 min with DHE and continuously perfused with buffer containing 1% or 10% CM. Buffer/unconditioned media and H_2O_2 (100 μM) perfusion were used as negative and positive controls, respectively. The real-time fluorescence measurement indicates that the surge of ROS level after H_2O_2 or 1%–10% CM stimulation was significantly higher than stimulation with buffer or 1%–10% unconditioned BHI media for 5 min (Figures 5A and 5B). In addition, cells stimulated with 1% or 10% CM presented increased DHE fluorescence in a similar manner. Because RyR blocking showed a protective effect on the mitochondrial Ca^{2+} homeostasis, we also aimed to test whether RyR blocking would diminish the damaging effects observed on αSyn homeostasis. As shown in Figures S8C and S8D, BHI CM elicited ROS generation, but this was efficiently reduced in cells previously incubated with dantrolene (Figures S8C and S8D). In addition, although RyR blocking prevented αSyn phosphorylation, no protective effect was observed regarding αSyn and GATA-2 expression (Figures S8E–S8H), suggesting that this phenomenon is RyR-mediated Ca^{2+} signaling independent.

As mentioned, stimuli that promote intracellular ROS formation and mitochondrial damage highly correlate with αSyn phosphorylation at Ser129, an event that may precede cell degeneration in PD (Perfeito et al., 2014). Previous observations have shown that both nigral and dorsal motor nucleus of the vagus nerve neurons present a high vulnerability to oxidative challenges (Musgrove et al., 2019). Because the nigro-vagal pathway that

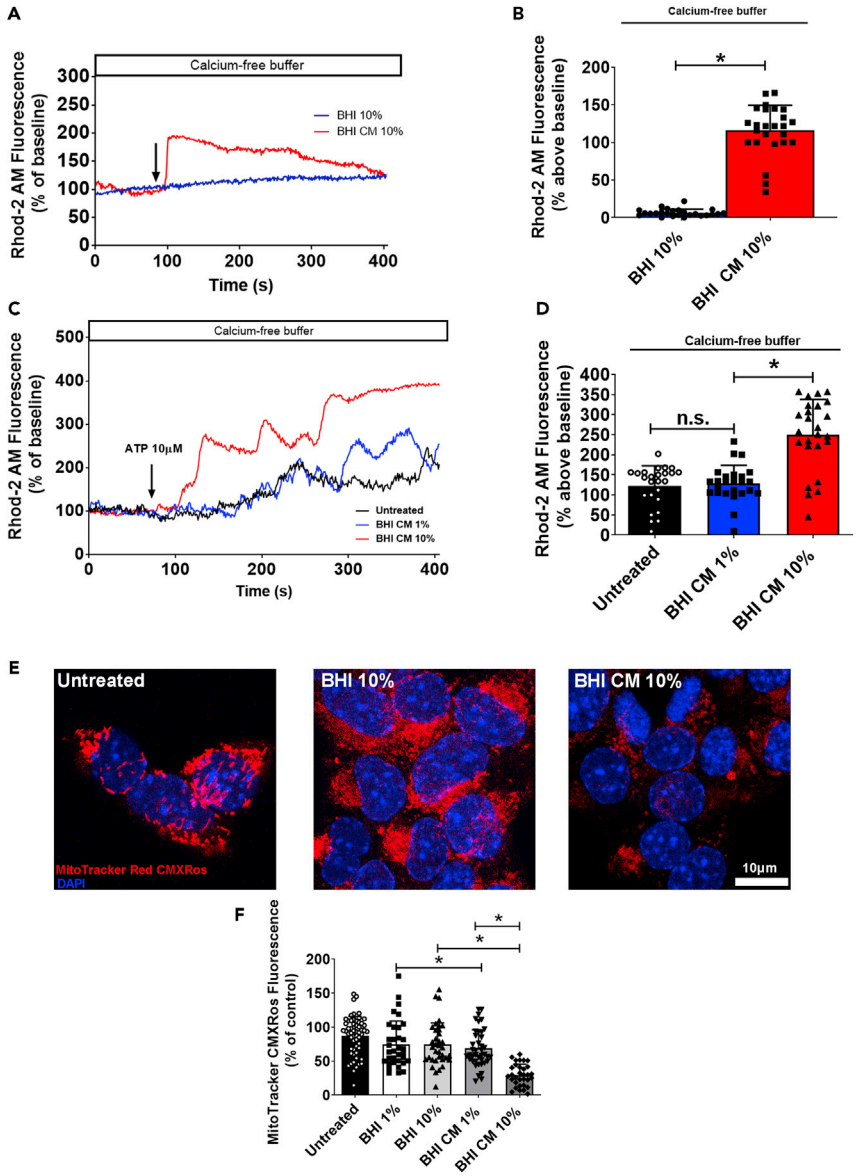

Figure 4. Increased mitochondrial Ca^{2+} uptake elicited by *Akkermansia muciniphila* conditioned media leads to mitochondrial stress and reduced $\Delta\Psi m$

(A) Representative time-course of mitochondrial Ca^{2+} signal. Cells were incubated with the mitochondrial Ca^{2+} indicator Rhod-2/AM and stimulated with 10% *A. muciniphila* conditioned medium (BHI CM) in the presence of Ca^{2+}-free buffer. The arrow indicates the time when culture medium was applied.

(B) Graphs show quantification of the peak of fluorescence following stimulation with 10% BHI CM.

(C) Representative time-course of mitochondrial Ca^{2+} signal of cells incubated for 48 h with 1%–10% *A. muciniphila* conditioned medium (BHI CM) and stimulated with 10 μM ATP in the presence of Ca^{2+}-free buffer. The arrow indicates the moment when culture medium was applied.

(D) Graphs show quantification of the peak of fluorescence following stimulation with ATP.

(E) Confocal images of STC-1 cells incubated for 48 h with 10% BHI CM and then stained with MitoTracker Red CMXRos (red). Nuclei were stained with DAPI (blue).

(F) Quantification of fluorescent signal in untreated and treated cells. Data in (A) and (C) represent a representative tracing recorded from one individual STC-1 cell of each group. Data in (B), (D), and (F) represented as mean ± SEM of three independent experiments in which at least 25 individual cells were analyzed. *$p < 0.05$ by unpaired Student's *t-test* See also Figure S8.

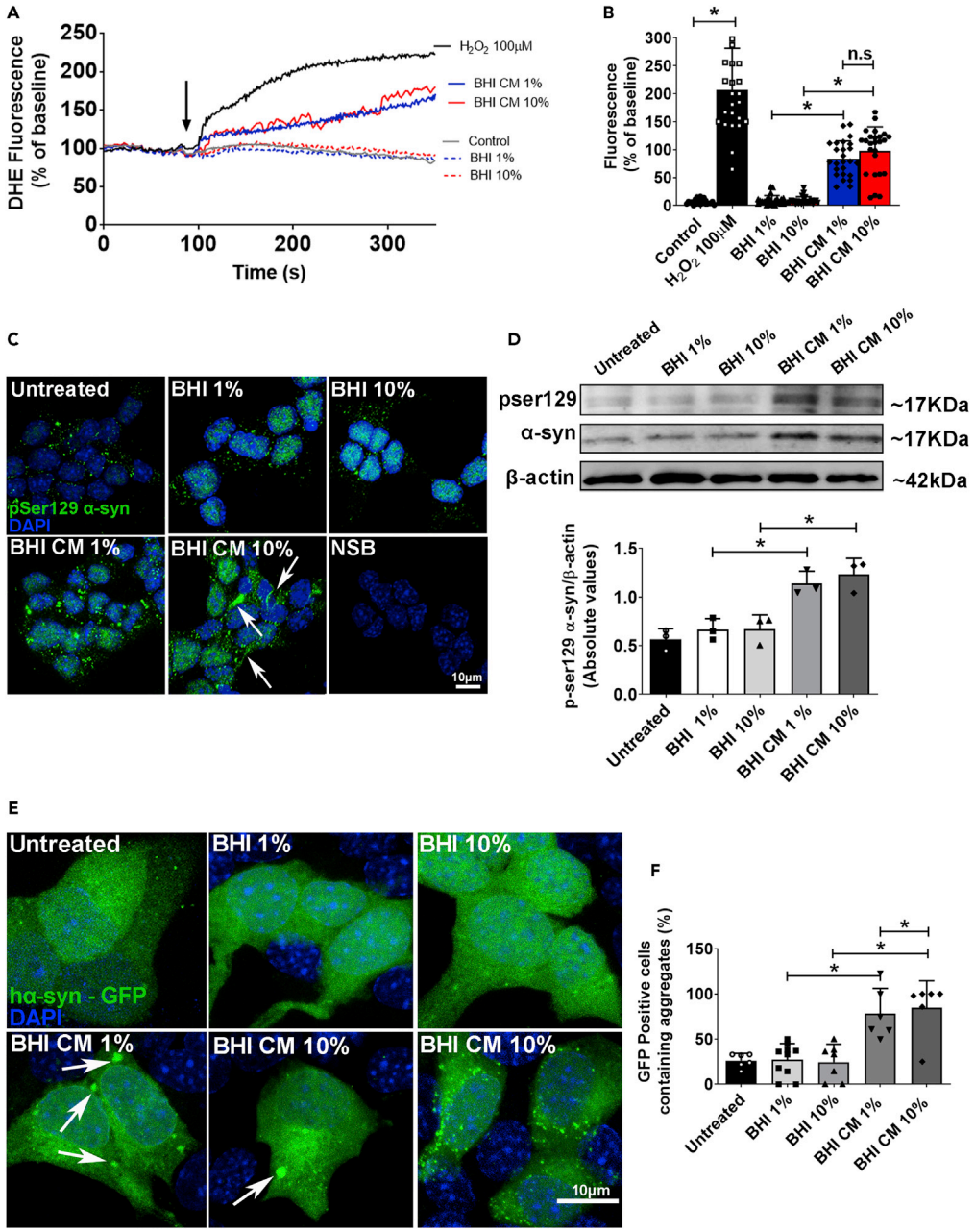

Figure 5. α-synuclein phosphorylation and aggregation as a result of increased intracellular levels of ROS due to *Akkermansia muciniphila* conditioned media treatment of enteroendocrine cells

(A) Time lapse of ROS production in STC-1 cells measured by DHE fluorescence intensity under confocal live imaging. 1% and 10% BHI or BHI CM was used as stimuli. 100 µM H_2O_2 was used as positive control.

(B) Quantitative summary of the effects of *A. muciniphila* conditioned and unconditioned media on ROS production. *p < 0.001 by unpaired Student's *t-test*.

(C) Confocal images of pSer129 αSyn staining (green) in STC-1 cells after 48-h incubation with 1%–10% conditioned (BHI CM) or unconditioned media (BHI) demonstrating increased phosphorylation of the protein. Nuclei were stained with DAPI (blue) and immunofluorescence control is shown as NSB (non-specific binding control). Arrows point to aberrant fibrillary-like structures. (Scale bar: 10 µm).

(D) Immunoblots (upper image) of total cell lysates showing the increased phosphorylation of αSyn on Ser129 (normalized against total αSyn) after 48-h incubation with 1/10% conditioned (BHI CM) or unconditioned media (BHI). Densitometric analysis shows phosphorylation of αSyn (pSer129) in 1%–10% BHI CM condition when compared to 1/10% BHI. *p < 0.05 by unpaired Student's *t-test*.

Figure 5. *Continued*

(E) Confocal images of hαSyn GFP-tagged plasmid transfected into STC-1 cells exhibits diffuse distribution in untreated or BHI-treated cells. Cells treated with 1%–10% BHI CM medium forms inclusions of different sizes (bottom images). (Scale bar: 10 μm).

(F) Graph shows the number of GFP-positive cells containing inclusions in each condition. *$p < 0.05$ by unpaired Student's *t-test*. Data in (A) represent a representative tracing recorded from one individual STC-1 cell of each group. Data in (B) and (F) represented as mean ± SEM of independent experiments in which at least 25 individual cells were analyzed in B and six slides for (F). Densitometric analysis of western blot (D) is derived from triplicates of three different experiments. See also Figure S8.

controls gastric tone and motility connect these brain regions, it raises the possibility that an oxidative injury may be relayed and possibly amplified through this anatomical and functional connection.

In order to evaluate whether increases in ROS levels induced by *A. muciniphila* CM could promote αSyn phosphorylation and aggregation, we incubated the cells for 48 h in the presence of CM or unconditioned BHI media analyzed them by immunofluorescence and Western blotting. Confocal microscopy images showed strong deposits of pSer129-αSyn in STC-1 cells incubated with 1% and 10% CM (Figure 5C). In addition, quantification by Western blotting showed a 2- to 3-fold increase of *p*-Ser129-αSyn in cells treated with the CM when normalized against total αSyn (Figure 5D).

To establish whether *A. muciniphila* CM-induced *p*-Ser129 αSyn might play a role on αSyn aggregation in our STC-1 cell model, we transfected cells with full-length human αSyn-GFP-tagged and incubated them with unconditioned or CM for 48 h. Unconditioned BHI media (1% or 10%) did not cause αSyn to form cellular inclusions. However, 1% and 10% CM led to the formation of small to large αSyn granules within the cytoplasm (Figure 5E). When we quantified the number of GFP-positive cells containing intracellular aggregates, we observed that over 50% of the cells stimulated with *A. muciniphila* CM contained αSyn granules (Figure 5F). Thereby, *A. muciniphila* CM grown in the absence of mucin induces intracellular αSyn aggregation in EECs *in vitro*.

Mitochondrial calcium buffering reverts the damaging effects to mitochondria and prevents α-synuclein aggregation

Inhibition of mitochondrial Ca^{2+} uptake was shown to diminish the oxidative stress in substantia nigra *pars compacta* dopaminergic neurons (SNpc DNs) suggesting that mitochondrial oxidative stress could also be due to mitochondrial Ca^{2+} overload (Guzman et al., 2010). Several lines of investigation point out to mitochondrial Ca^{2+} imbalance as a key factor to be modulated in order to control the progression of PD. We previously showed that RyR blocking leads to a protective effect on the mitochondrial Ca^{2+} homeostasis in cells submitted do BHI CM treatment (Figures S8A and S8B). To further explore the role of mitochondrial Ca^{2+} in αSyn pathology in EECs treated with the protein-enriched fraction of *A.muciniphila* CM and in order to observe whether modulating mitochondrial Ca^{2+} in these cells could reverse intracellular ROS generation and αSyn aggregation, we transfected the cells with parvalbumin (PV) fused to a mitochondrial-targeting sequence (MTS) and GFP (Guerra et al., 2011). Parvalbumin (PV) is a cytosolic Ca^{2+}-binding protein of the large EF-hand protein family, involved in intracellular Ca^{2+} regulation and buffering. GFP targeted to the mitochondrial matrix was used as a control (MTS-GFP) (Figure 6A).

One or 10% BHI CM elicited a robust increase in mitochondrial Ca^{2+} in cells expressing MTS-GFP alone, but this was reduced by approximately 90% in cells expressing PV in mitochondria (Figures 6B and 6C). These results demonstrated that PV-MTS-GFP was correctly targeted to the mitochondrial matrix and efficiently buffered mitochondrial Ca^{2+} overload driven by stimulation with *A. muciniphila* CM.

Once mitochondrial Ca^{2+} was buffered, the next set of experiments aimed to observe whether the damaging effects caused by *A. muciniphila* CM could be prevented. When we stimulated the cells expressing PV-MTS construct with 1% and 10% BHI CM, the increase in intracellular ROS was significantly suppressed (Figures 6D and 6E) indicating that mitochondrial Ca^{2+} buffering prevents intracellular oxidative stress.

To test the effect of mitochondrial Ca^{2+} on Ser129-phosphorylation of αSyn induced by *A. muciniphila* CM, we incubated the transfected cells with 1% or 10% CM for 48 h. Total cell lysate evaluated by Western

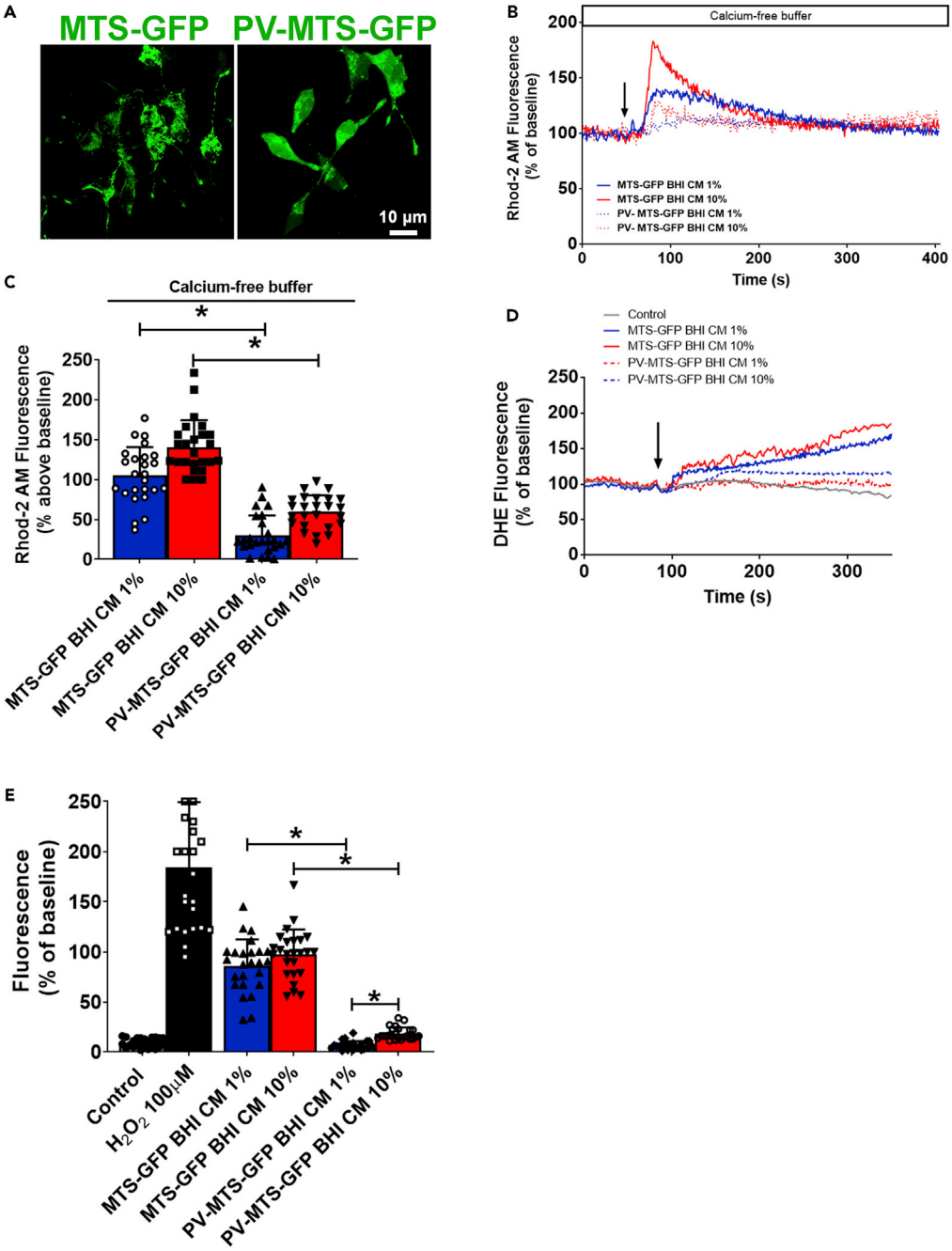

Figure 6. Mitochondrial Ca^{2+} buffering reduces intracellular ROS levels elicited by *Akkermansia muciniphila* conditioned medium

(A) Confocal images of STC-1 cells transfected with mitochondrial parvalbumin (PV) expression and control vectors showing the expression and mitochondrial localization of targeted PV-MTS-GFP and MTS-GFP fusion proteins. Scale bar = 10 μM.

(B) Representative changes in mitochondrial Ca^{2+} signals over time are shown. Cells transfected with the indicated vectors were loaded with Rhod-2/AM and stimulated with 1%–10% unconditioned (BHI) or conditioned medium (BHI-CM) (arrow). Ca^{2+} signals were attenuated in cells expressing PV in mitochondria.

(C) Peak Ca^{2+} signals were observed in three separate experiments for STC-1 cells transfected with MTS-GFP, and cells transfected with PV-MTS-GFP. *$p < 0.05$ by unpaired Student's *t-test*.

(D) Representative changes in intracellular ROS levels over time are shown. Cells transfected with the indicated vectors were loaded with DHE and induced by 1/10% unconditioned (BHI) or conditioned medium (BHI-CM) (arrow). DHE fluorescence intensity was significantly reduced in cells expressing PV-MTS-GFP fusion protein.

Figure 6. *Continued*
(E) Peak ROS signals were observed in three separate experiments for STC-1 cells transfected with MTS-GFP, and cells transfected with PV-MTS-GFP stimulated with each represented condition. *p < 0.05 by unpaired Student's *t-test*. Data in (B) and (D) represent a representative tracing recorded from one individual STC-1 cell of each group. Data in (C) and (E) represented as mean ± SEM of three independent experiments in which at least 25 individual cells were analyzed.

blotting showed that levels of Ser129-phosphorylated αSyn significantly decreased in PV-MTS expressing cells when compared with control cells (MTS-GFP) (Figures 7A and 7B). However, no effect was observed in the total expression level of αSyn, which remained higher when compared to untreated cells (Figures 7A and 7C).

We then extended our observation that mitochondrial Ca^{2+} buffering can suppress intracellular ROS generation, αSyn phosphorylation, and the formation of αSyn aggregates. Hence, we double-transfected cells with the PV-MTS-GFP construct and mCherry-tagged human αSyn. A large number of αSyn aggregates were observed in cells expressing the control construct (MTS-GFP) after 48 h of treatment with 1% or 10% CM. However, the number of αSyn aggregates in cells expressing the PV-MTS-GFP constructed was markedly reduced (Figures 7D and 7E).

Taking together, these findings provide evidence on the mechanism by which *A. muciniphila* CM induces αSyn aggregation in EECs *in vitro*.

Oral administration of *A. muciniphila* to aged mice leads to αSyn aggregation in CCK-positive enteroendocrine cells

So far, our results showed that the protein fraction of *A.muciniphila* CM grown in the absence of mucin induces mitochondrial stress and ROS generation which in turn led to αSyn aggregation. In addition, previous studies have shown that aged mice have impaired mucus barrier in the colon and ileum and this thinner mucus layer was associated with increased bacterial penetrability and contact with the epithelium (Elderman et al., 2017; Sovran et al., 2019). Indeed, when we dosed mucin levels in the feces of aged mice (18–20 months old), we found it to be dramatically decreased when compared to young mice (2 months old) (Figure S9A). Therefore, we wondered whether the increased levels of *A.muciniphila* in aged mice could be a trigger to αSyn pathology in the gut. To assess if *A.muciniphila* could cause motor deficits, we treated aged mice with bacterial cells (AKK group) for 28 continuous days (Figure S9B). After 28 days of oral administration, AKK group did not exhibit alteration in body weight but presented significantly higher number of *A. muciniphila* 16S rRNA copies in stool (Figures S9C and S9D).

We used three measures of gross motor function: time to cross a challenging beam, the cylinder test, and wire hanging. In none of the test we observed differences between control and AKK group (Figures S9E–S9G). Utilizing an antibody that recognizes only conformation-specific αSyn aggregates and fibrils, we performed dot blot analysis for aggregated αSyn in total protein extract from ileum of control and *A.muciniphila*-treated animals and observe similarly low levels of αSyn aggregation in both groups (Figures 8A and 8B). Interestingly, by immunofluorescence, we observe αSyn aggregation in cholecystokinin (CCK)-positive EECs (Figures 8C and 8D). In addition, the number of CCK-positive cells containing αSyn aggregates in AKK group was ~4 times higher when compared to control animals which barely presented αSyn-aggregate-containing cells (Figure 8E). These data suggest that *A.muciniphila*, when exposed to a mucin-deprived environment, regulates pathways that promote αSyn aggregation and/or prevent the clearance of insoluble protein aggregates in EECs in the conditions we showed here.

DISCUSSION

Parkinson disease is a growing health concern for an ever-aging population. Although genetic risks have been identified, environmental influences and gene-environment interactions are so far considered responsible for most PD cases (Nalls et al., 2014). Besides the plethora of neurological and motor symptoms, patients with PD present prominent gut manifestations (Abbott et al., 2001; Adams-Carr et al., 2016; Chaudhuri et al., 2006; Jost, 2010; Klingelhoefer and Reichmann, 2015; Mertsalmi et al., 2017).

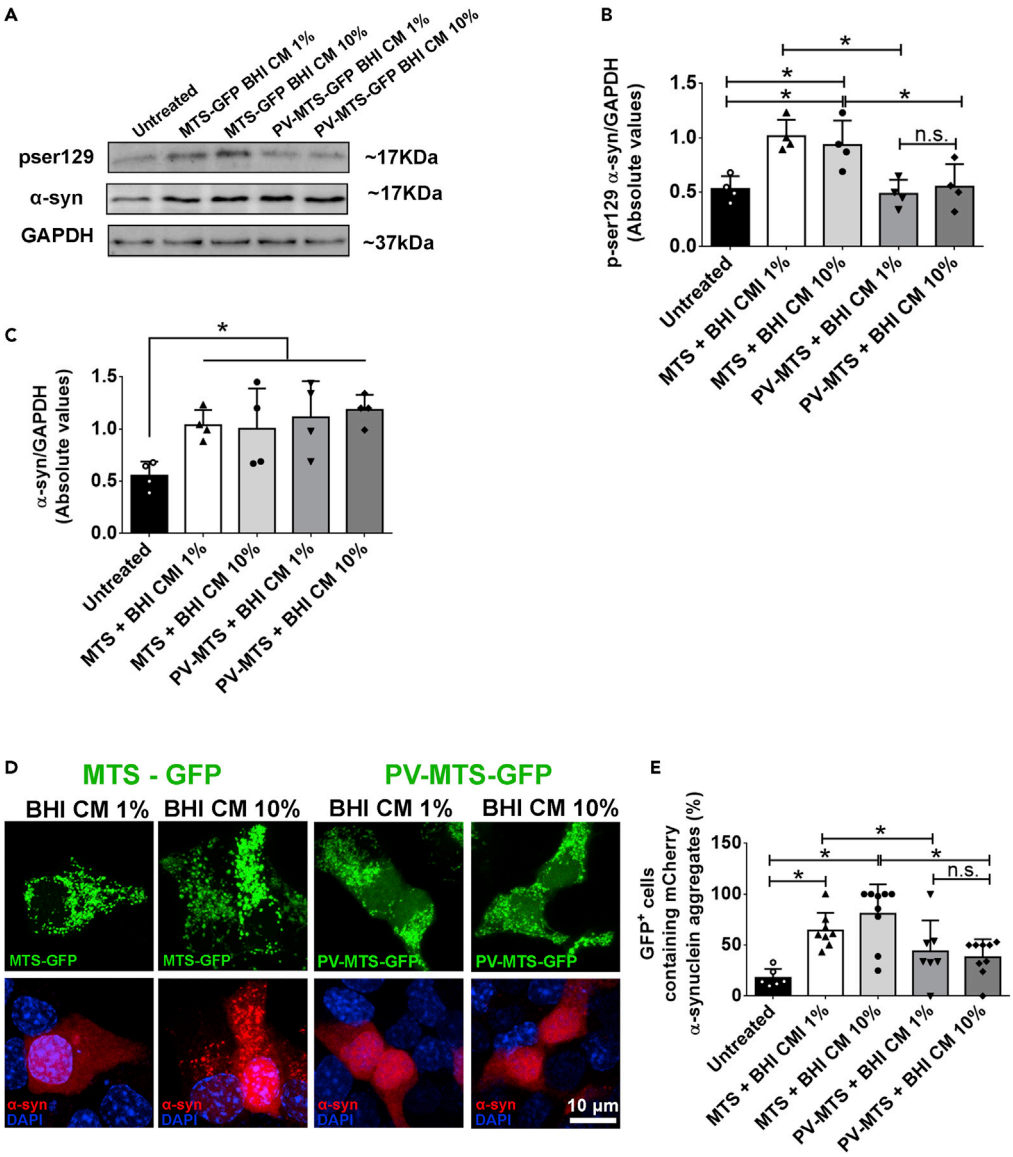

Figure 7. α-synuclein phosphorylation and aggregation induced by *Akkermansia muciniphila* conditioned medium are prevented due to mitochondrial Ca^{2+} buffering

(A) Immunoblots (upper image) of total cell lysates from PV-MTS-GFP or MTS-GFP transfected cells showing a decrease in αSyn phosphorylation on Ser129 after 48-h incubation with 1%–10% conditioned (BHI CM) or unconditioned media (BHI).

(B) Densitometric analysis shows that mitochondrial Ca^{2+} buffering reduced αSyn phosphorylation in 1%–10% BHI CM condition when compared to cells expressing MTS-GFP fusion protein. *$p < 0.05$ by two-way Student's *t-test*.

(C) Densitometric analysis shows that mitochondrial Ca^{2+} buffering did not reduce αSyn expression induced by 1/10% BHI CM condition when compared to cells expressing MTS-GFP fusion protein. *$p < 0.05$ by two-way Student's *t-test*.

(D) Confocal images of STC-1 cells co-transfected with PV-MTS-GFP and αSyn-mCherry tagged construct show reduced number of intracellular αSyn aggregates after 48 h incubation with 1%–10% BHI CM. (scale bar: 10μM).

(E) Quantification of the number of GFP-positive cells containing mCherry-tagged αSyn aggregates. Data are expressed as percentage of total GFP-positive cells per image. *$p < 0.05$; Ns, not significant by unpaired Student's *t-test*.

Densitometric analysis of western blot (B) and (C) are derived from triplicates of three different experiments. Data in (E) represented as the mean ± SEM of at least three independent experiments in which at least six individual slides were analyzed.

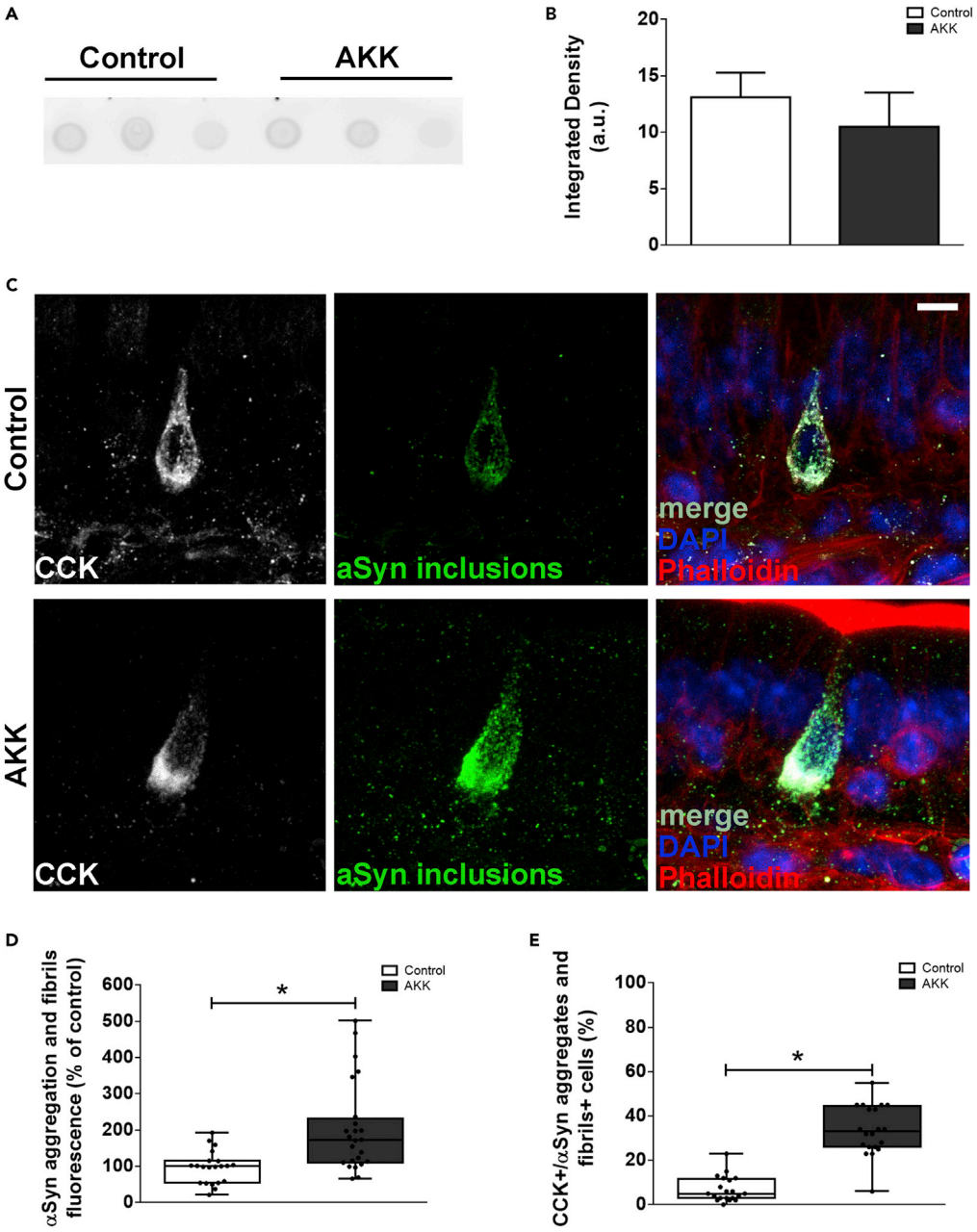

Figure 8. Commensal gut *Akkermansia muciniphila* induces α-synuclein aggregation in enteroendocrine cells

(A) Aggregate-specific aSyn dot blots derived from total ileum homogenate of aged mice. Each dot is representative of a piece of tissue from one animal.

(B) Densitometry quantification of dot blots in (A).

(C) 3D z stack image of a 150μm section of the ileum of aged mice treated with PBS or with mucin-free cultivated *A. muciniphila* (AKK) for 28 days. CCK-positive EECs are stained for anti-CCK (white), specific antibody for αSyn-aggregates (green), actin cytoskeleton (phalloidin, red), and DAPI.

(D) Quantification of αSyn aggregates and fibrils fluorescence (% of control).

(E) Quantification of the number of CCK-positive cells containing αSyn aggregates and fibrils in control and AKK-treated mice. Data are represented as mean ± SEM Each dot represents the mean fluorescence of at least 15 cells per slice (at least three slices of five individual animals). Scale bar = 10 μm. See also Figure S9.

Aggregates of the protein αSyn are a hallmark of PD. Interestingly, αSyn pathology in PD is not limited to the brain. It was also observed in the peripheral nervous system, including the enteric nervous system (Wakabayashi et al., 2010). Therefore, the interaction between the gut microbiota, EECs, and αSyn aggregation in PD is receiving increasing attention. The idea that αSyn aggregation process is initiated in the gut following continuous gastrointestinal symptoms aggravation and spreading to the nervous system in a prion-like manner has gathered significant force in recent years. Some pathophysiological evidence helps to support this notion: αSyn inclusions appear earlier in the enteric nervous system and the glossopharyngeal and vagal nerves (Braak et al., 2003a, 2003b); and vagotomized individuals are at reduced risk for PD (Sampson et al., 2016). In addition, injection of αSyn fibrils into the gut tissue of healthy rodents seemed sufficient to induce disease within the vagus nerve and brainstem (Kim et al., 2019).

The finding that EECs connect to nerves raises an array of possibilities for how nutrients, bacteria, toxins, and potential pathogens gain access to and communicate with the nervous system. The discovery of αSyn in EECs, which are directly exposed to *A. muciniphila* secreted proteins in the gut lumen and connected to enteric nerves, provides a location in which misassemble and spread of αSyn could initiate (Chandra et al., 2017). However, the knowledge of how αSyn aggregation initiates in the gut and spreads to the CNS via retrograde transmission and whether the gut microbiome could directly trigger this process remains controversial (Sampson et al., 2016).

The specific mechanisms by which gut bacteria promote αSyn-mediated pathophysiology are likely diverse, complex, and poorly explored. Nonetheless, in this work, we have identified that mitochondrial Ca^{2+} overload in an enteroendocrine cell model led by the CM of a commensal gut bacterium *A. muciniphila* is a molecular pathway by which αSyn homeostasis can be disturbed in EECs *in vitro*, providing experimental support for a gut-microbial connection to PD.

Since its discovery in 2004, *A. muciniphila* (Derrien et al., 2004) has gathered a great amount of scientific attention. It has been shown that intestinal *Akkermansia* abundance is significantly reduced in many metabolic disorders, including type 2 diabetes, obesity, and dyslipidemia (Derrien et al., 2017). Therefore, this has stimulated several studies in order to investigate *Akkermansia* supplementation. Evidence shows some beneficial effects of *Akkermansia* supplementation. This approach was shown to restore epithelial mucosal integrity, reduce weight gain and fat accumulation in the liver, improve glucose tolerance, and to reduce inflammation and metabolic endotoxemia in animal models of diabetes and obesity (Derrien et al., 2004; Plovier et al., 2017). Moreover, in opposition to previous findings that suggested a detrimental role of the increased levels of *A. muciniphila* in patients with multiple sclerosis (Berer et al., 2017; Cekanaviciute et al., 2017), it was recently shown that this bacterium was linked to lower disability, suggesting a beneficial role further corroborated in animal model for autoimmune encephalitis (Cox et al., 2021).

However, we cannot rule out recent reports showing that alteration in gut microbiota is associated with PD. Several lines of evidence suggest that patients with PD present strong gut dysbiosis with remarkable abundance of *A. muciniphila* which is consistently high in PD stool samples (Baldini et al., 2020; Bedarf et al., 2017; Heintz-Buschart et al., 2018; Hill-Burns et al., 2017; Li et al., 2017; Lin et al., 2019; Mertsalmi et al., 2017; Nishiwaki et al., 2020; Unger et al., 2016; Vidal-Martinez et al., 2020). Whether this is detrimental or not remains to be addressed.

In this work, we showed that the proteins obtained from *A. muciniphila* CM cultivated in mucin-free medium induce RyR-dependent ER Ca^{2+} release *in vitro*. This persistent Ca^{2+}-mediated signals is followed by increased mitochondrial Ca^{2+} uptake in STC-1 cells, which in turn culminates with αSyn phosphorylation and aggregation.

This phenomenon related to mucin presence in culture medium leads us to the fact that in order to maintain the mammalian intestinal homeostasis with the microbiota, a key element is to minimize and regulate contact between luminal microorganisms and the intestinal epithelial cell surface. In the gut, physical separation of bacteria and the epithelium is greatly accomplished by secretion of mucus, antimicrobial proteins, and IgA into the lumen (Macpherson et al., 2000; Macpherson and Harris, 2004). Interestingly, it was previously shown that aged mice (15–19 months old) have an impaired mucus barrier in the colon and ileum

accompanied by major changes in the fecal microbiota composition, a fact that has also been observed in humans (Elderman et al., 2017; Sovran et al., 2019). Therefore, besides changing the microbiome pattern of secretion (Figure 1), a decrease on mucus barrier thickness leads to increased contact of gut bacteria and their secreted components with the intestinal epithelium that could therefore modulate gut cells homeostasis, especially misbalancing intracellular Ca^{2+} dynamics.

An emerging, key pathological feature in neurons affected by PD is the global dysregulation of Ca^{2+} homeostasis (Zaichick et al., 2017). Ca^{2+} handling through contact sites between the ER and mitochondria (mitochondria-associated ER membranes – MAMs) have attracted great attention in the study of cell homeostasis and dysfunction, especially in the context of neurodegenerative disorders. Emerging evidence suggests that the abnormality and dysfunction of MAMs have been involved in a number of neurodegenerative disorders including Alzheimer disease, amyotrophic lateral sclerosis, and Parkinson disease (Gautier et al., 2016; Hedskog et al., 2013; Liu and Zhu, 2017). Also, increased intracellular Ca^{2+} levels alter Ca^{2+} handling in intracellular organelles such as the ER and mitochondria which may potentiate pathological effects (Ludtmann and Abramov, 2018). Indeed, Ca^{2+} uptake into the mitochondria is a key mechanism by which cells maintain intracellular Ca^{2+} homeostasis (Dey et al., 2020; Vos et al., 2010). However, excessive mitochondrial Ca^{2+} uptake or impaired Ca^{2+} efflux results in ROS production (Luongo et al., 2017; Reynolds and Hastings, 1995) and disruption of membrane potential inducing neuronal cell death, an important indicator of several different neurological disorders including Alzheimer disease (AD) and PD. Moreover, it has been suggested that impaired mitochondrial biogenesis, Ca^{2+} buffering, and oxidative stress may precede the development of PD and AD pathology (Jadiya et al., 2019; Kandimalla et al., 2018; Pratico et al., 2001; Rani and Mondal, 2020). Recent studies indicate that increased intracellular-free Ca^{2+} and oxidative stress synergistically augment the number of cytoplasmic αSyn-enriched aggregates *in vitro* and *in vivo* (Goodwin et al., 2013). In addition, it is also known that αSyn aggregates trigger increased mitochondrial Ca^{2+} transient and then leads to oxidative stress (Ganjam et al., 2019; Scudamore and Ciossek, 2018). Thus, an increase in oxidative stress can cause αSyn aggregation which can also induce further oxidative stress within the cell creating a positive feedback loop.

Although very clear for neuronal cells, we show here that this cascade of events is also triggered in EECs stimulated by *A. muciniphila*-secreted proteins. The outcome of this persistent Ca^{2+} mishandling is very similar to what has already been reported for neurons in PD. Additionally, since αSyn-containing EECs directly connect to enteric nerve terminals forming a neural circuit between the gut and the nervous system, influences in the gut lumen affect αSyn folding in the EECs which can then propagate to the nervous system. Hence, using an *in vitro* approach, we offer some mechanistic insights of how misfolded αSyn could be generated in EECs. However, it is important to highlight that whether this might be a causative role for sporadic PD should be addressed in more complex models.

Limitations of the study

In this work, we showed that the composition of the protein fraction of *A. muciniphila* CM is dependent on mucin metabolism. In addition, only mucin-free CM induces an IP_3-independent ER-calcium release in EECs *in vitro*. This Ca^{2+} release is triggered by direct activation of RyR leading to increased mitochondrial Ca^{2+} uptake which leads to ROS generation and αSyn aggregation in these cells. However, it remains obscure whether the intracellular events observed here in our *in vitro* condition would also happen in more physiological models. If so, which specific protein(s) present in the *A.muciniphila* CM is (are) the causative role for this cascade of events should also be addressed. Further characterization of these proteins and their relevance for neurological conditions in more complex models will be fundamental to unveil the consequences of *A.muciniphila* dysbiosis. In addition, it remains to be addressed whether αSyn aggregates in CCK-positive EECs from the mouse duodenum might be transferred to enteric neurons and therefore trigger αSyn pathology progression.

ETHICS APPROVAL

The experiments were conducted according to the National Institutes of Health Guidelines for the Care and Use of Laboratory Animals (NIH publications No. 8023, revised 1978). All experiments with animals were approved by the Institutional Committee of Animal Use & Protection (CEUA 92-B).

STAR★METHODS

Detailed methods are provided in the online version of this paper and include the following:

- KEY RESOURCES TABLE
- RESOURCE AVAILABILITY
  - Lead contact
  - Materials availability
  - Data and code availability
- EXPERIMENTAL MODELS AND SUBJECT DETAILS
  - Cell lines
  - Animals
- METHOD DETAILS
  - Fecal microbial community analysis
  - Quantification of fecal mucin
  - Behavioral tests
  - Conditioned media collection
  - Mass spectrometry
  - ^{1}H NMR spectra acquisition
  - Assignment and quantification of the metabolites
  - Plasmids and transfection
  - Immunofluorescence
  - Cell viability
  - Immunoblotting
  - Cytosolic and mitochondrial calcium measurements
  - Detection of reactive oxygen species (ROS)
  - Evaluation of mitochondrial membrane potential
  - Immunohistofluorescence
- QUANTIFICATION AND STATISTICAL ANALYSIS

SUPPLEMENTAL INFORMATION

Supplemental information can be found online at https://doi.org/10.1016/j.isci.2022.103908.

ACKNOWLEDGMENTS

We thank Dr. Maria de Fátima Leite (UFMG, Brazil) for valuable comments on this manuscript. We thank Dr. Silvana Rocco, Dr. Maurício Sforça, and Dr. Marcos Rodrigo Alborghetti (LNBio, Brazil) for helping with NMR data collection, analysis, and interpretation. The authors would like to acknowledge support of INFABIC, Unicamp and the Brazilian Biorenewables National Laboratory (LNBR – CNPEM) for providing access to its facilities. We also acknowledge the Mass Spectrometry Laboratory and Nuclear Magnetic Resonance Laboratory at Brazilian Biosciences National Laboratory (LNBio), Brazilian Center for Research in Energy and Materials (CNPEM), Campinas, Brazil, for their support with the mass spectrometry and NMR analysis. This work was supported by Fundação de Amparo à Pesquisa do Estado de São Paulo (FAPESP) under the grant numbers 2018/20014-0 and 2019/24511-0. This work was also supported by Fondo de Financiamiento de Centros de Investigación en Áreas Prioritarias (ANID/FONDAP/15150012). INFABIC is co-funded by FAPESP (2014/50938-8) and Conselho Nacional de Desenvolvimento Científico e Tecnológico (CNPq) (465699/2014-6).

AUTHOR CONTRIBUTIONS

Conceptualisation, MCF and DPAN; Formal Analysis, DPAN, BPG, and MCF; Investigation, DPAN, BPB, JVPG, KT, PV, and CCCT; Resources, CCCT and MCF; Writing, DPAN, HFC, CGB, and MCF; Funding Acquisition, HFC and MCF.

DECLARATION OF INTEREST

The authors declare no competing interests.

INCLUSION AND DIVERSITY

One or more of the authors of this paper self-identifies as an underrepresented ethnic minority in science.
One or more of the authors of this paper self-identifies as a member of the LGBTQ + community.

Received: September 29, 2021
Revised: December 6, 2021
Accepted: February 8, 2022
Published: March 18, 2022

REFERENCES

Abbott, R.D., Petrovitch, H., White, L.R., Masaki, K.H., Tanner, C.M., Curb, J.D., Grandinetti, A., Blanchette, P.L., Popper, J.S., and Ross, G.W. (2001). Frequency of bowel movements and the future risk of Parkinson's disease. Neurology *57*, 456–462.

Adams-Carr, K.L., Bestwick, J.P., Shribman, S., Lees, A., Schrag, A., and Noyce, A.J. (2016). Constipation preceding Parkinson's disease: a systematic review and meta-analysis. J. Neurol. Neurosurg. Psychiatry *87*, 710–716.

Alvarenga, E.C., Fonseca, M.C., Carvalho, C.C., Florentino, R.M., Franca, A., Matias, E., Guimaraes, P.B., Batista, C., Freire, V., Carmona, A.K., et al. (2016). Angiotensin converting enzyme regulates cell proliferation and migration. PLoS ONE *11*, e0165371.

Baldini, F., Hertel, J., Sandt, E., Thinnes, C.C., Neuberger-Castillo, L., Pavelka, L., Betsou, F., Kruger, R., Thiele, I., and Consortium, N.-P. (2020). Parkinson's disease-associated alterations of the gut microbiome predict disease-relevant changes in metabolic functions. BMC Biol. *18*, 62.

Bedarf, J.R., Hildebrand, F., Coelho, L.P., Sunagawa, S., Bahram, M., Goeser, F., Bork, P., and Wullner, U. (2017). Functional implications of microbial and viral gut metagenome changes in early stage L-DOPA-naive Parkinson's disease patients. Genome Med. *9*, 39.

Bekris, L.M., Mata, I.F., and Zabetian, C.P. (2010). The genetics of Parkinson disease. J. Geriatr. Psychiatry Neurol. *23*, 228–242.

Berer, K., Gerdes, L.A., Cekanaviciute, E., Jia, X., Xiao, L., Xia, Z., Liu, C., Klotz, L., Stauffer, U., Baranzini, S.E., et al. (2017). Gut microbiota from multiple sclerosis patients enables spontaneous autoimmune encephalomyelitis in mice. Proc. Natl. Acad. Sci. U S A *114*, 10719–10724.

Bernheimer, H., Birkmayer, W., Hornykiewicz, O., Jellinger, K., and Seitelberger, F. (1973). Brain dopamine and the syndromes of Parkinson and Huntington. Clinical, morphological and neurochemical correlations. J. Neurol. Sci. *20*, 415–455.

Bilodeau, M.L., Boulineau, T., Greulich, J.D., Hullinger, R.L., and Andrisani, O.M. (2001). Differential expression of sympathoadrenal lineage-determining genes and phenotypic markers in cultured primary neural crest cells. In Vitro Cell Dev. Biol. Anim. *37*, 185–192.

Bohorquez, D.V., Shahid, R.A., Erdmann, A., Kreger, A.M., Wang, Y., Calakos, N., Wang, F., and Liddle, R.A. (2015). Neuroepithelial circuit formed by innervation of sensory enteroendocrine cells. J. Clin. Invest. *125*, 782–786.

Braak, H., and Del Tredici, K. (2009). Neuroanatomy and pathology of sporadic Parkinson's disease. Adv. Anat. Embryol. Cell Biol. *201*, 1–119.

Braak, H., Del Tredici, K., Rub, U., de Vos, R.A., Jansen Steur, E.N., and Braak, E. (2003a). Staging of brain pathology related to sporadic Parkinson's disease. Neurobiol. Aging *24*, 197–211.

Braak, H., Rub, U., Gai, W.P., and Del Tredici, K. (2003b). Idiopathic Parkinson's disease: possible routes by which vulnerable neuronal types may be subject to neuroinvasion by an unknown pathogen. J. Neural Transm. *110*, 517–536.

Calvo-Rodriguez, M., Hou, S.S., Snyder, A.C., Kharitonova, E.K., Russ, A.N., Das, S., Fan, Z., Muzikansky, A., Garcia-Alloza, M., Serrano-Pozo, A., et al. (2020). Increased mitochondrial calcium levels associated with neuronal death in a mouse model of Alzheimer's disease. Nat. Commun. *11*, 2146.

Cekanaviciute, E., Yoo, B.B., Runia, T.F., Debelius, J.W., Singh, S., Nelson, C.A., Kanner, R., Bencosme, Y., Lee, Y.K., Hauser, S.L., et al. (2017). Gut bacteria from multiple sclerosis patients modulate human T cells and exacerbate symptoms in mouse models. Proc. Natl. Acad. Sci. U S A *114*, 10713–10718.

Chandra, R., Hiniker, A., Kuo, Y.M., Nussbaum, R.L., and Liddle, R.A. (2017). alpha-Synuclein in gut endocrine cells and its implications for Parkinson's disease. JCI Insight *2*, e92295.

Chaudhuri, K.R., Healy, D.G., Schapira, A.H., and National Institute for Clinical, E. (2006). Non-motor symptoms of Parkinson's disease: diagnosis and management. Lancet Neurol. *5*, 235–245.

Collado, M.C., Derrien, M., Isolauri, E., de Vos, W.M., and Salminen, S. (2007). Intestinal integrity and Akkermansia muciniphila, a mucin-degrading member of the intestinal microbiota present in infants, adults, and the elderly. Appl. Environ. Microbiol. *73*, 7767–7770.

Cox, L.M., Maghzi, A.H., Liu, S., Tankou, S.K., Dhang, F.H., Willocq, V., Song, A., Wasen, C., Tauhid, S., Chu, R., et al. (2021). Gut microbiome in progressive multiple sclerosis. Ann. Neurol. *89*, 1195–1211.

Davie, C.A. (2008). A review of Parkinson's disease. Br. Med. Bull. *86*, 109–127.

de Lau, L.M., and Breteler, M.M. (2006). Epidemiology of Parkinson's disease. Lancet Neurol. *5*, 525–535.

Derrien, M., Belzer, C., and de Vos, W.M. (2017). Akkermansia muciniphila and its role in regulating host functions. Microb. Pathogenesis *106*, 171–181.

Derrien, M., Vaughan, E.E., Plugge, C.M., and de Vos, W.M. (2004). Akkermansia muciniphila gen. nov., sp. nov., a human intestinal mucin-degrading bacterium. Int. J. Syst. Evol. Microbiol. *54*, 1469–1476.

Desai, M.S., Seekatz, A.M., Koropatkin, N.M., Kamada, N., Hickey, C.A., Wolter, M., Pudlo, N.A., Kitamoto, S., Terrapon, N., Muller, A., et al. (2016). A dietary fiber-deprived gut microbiota degrades the colonic mucus barrier and enhances pathogen susceptibility. Cell *167*, 1339–1353.e1321.

Dey, K., Bazala, M.A., and Kuznicki, J. (2020). Targeting mitochondrial calcium pathways as a potential treatment against Parkinson's disease. Cell Calcium *89*, 102216.

Di Lisa, F., and Bernardi, P. (2009). A CaPful of mechanisms regulating the mitochondrial permeability transition. J. Mol. Cell Cardiol. *46*, 775–780.

Divecha, N., Banfic, H., and Irvine, R.F. (1991). The polyphosphoinositide cycle exists in the nuclei of Swiss 3T3 cells under the control of a receptor (for IGF-I) in the plasma membrane, and stimulation of the cycle increases nuclear diacylglycerol and apparently induces translocation of protein kinase C to the nucleus. EMBO J. *10*, 3207–3214.

Elderman, M., Sovran, B., Hugenholtz, F., Graversen, K., Huijskes, M., Houtsma, E., Belzer, C., Boekschoten, M., de Vos, P., Dekker, J., et al. (2017). The effect of age on the intestinal mucus thickness, microbiota composition and immunity in relation to sex in mice. PloS One *12*, e0184274.

Fleming, S.M., Ekhator, O.R., and Ghisays, V. (2013). Assessment of sensorimotor function in mouse models of Parkinson's disease. J. Vis. Exp. 50303.

Fonseca, M.C., Franca, A., Florentino, R.M., Fonseca, R.C., Lima Filho, A.C.M., Vidigal, P.T.V., Oliveira, A.G., Dubuquoy, L., Nathanson, M.H., and Leite, M.F. (2018). Cholesterol-enriched membrane microdomains are needed for insulin signaling and proliferation in hepatic cells. Am. J. Physiol. Gastrointest. Liver Physiol. *315*, G80–G94.

Gafni, J., Munsch, J.A., Lam, T.H., Catlin, M.C., Costa, L.G., Molinski, T.F., and Pessah, I.N. (1997). Xestospongins: potent membrane permeable blockers of the inositol 1,4,5-trisphosphate receptor. Neuron *19*, 723–733.

Gagic, D., Ciric, M., Wen, W.X., Ng, F., and Rakonjac, J. (2016). Exploring the secretomes of microbes and microbial communities using filamentous phage display. Front. Microbiol. *7*, 429.

Ganjam, G.K., Bolte, K., Matschke, L.A., Neitemeier, S., Dolga, A.M., Hollerhage, M., Hoglinger, G.U., Adamczyk, A., Decher, N., Oertel, W.H., et al. (2019). Mitochondrial damage by alpha-synuclein causes cell death in human dopaminergic neurons. Cell Death Dis. *10*, 865.

Gautier, C.A., Erpapazoglou, Z., Mouton-Liger, F., Muriel, M.P., Cormier, F., Bigou, S., Duffaure, S., Girard, M., Foret, B., Iannielli, A., et al. (2016). The endoplasmic reticulum-mitochondria interface is perturbed in PARK2 knockout mice and patients with PARK2 mutations. Hum. Mol. Genet. *25*, 2972–2984.

Goodwin, J., Nath, S., Engelborghs, Y., and Pountney, D.L. (2013). Raised calcium and oxidative stress cooperatively promote alpha-synuclein aggregate formation. Neurochem. Int. *62*, 703–711.

Grander, C., Adolph, T.E., Wieser, V., Lowe, P., Wrzosek, L., Gyongyosi, B., Ward, D.V., Grabherr, F., Gerner, R.R., Pfister, A., et al. (2018). Recovery of ethanol-induced Akkermansia muciniphila depletion ameliorates alcoholic liver disease. Gut *67*, 891–901.

Greenamyre, J.T., and Hastings, T.G. (2004). Biomedicine. Parkinson's–divergent causes, convergent mechanisms. Science *304*, 1120–1122.

Greenland, J.C., Williams-Gray, C.H., and Barker, R.A. (2019). The clinical heterogeneity of Parkinson's disease and its therapeutic implications. Eur. J. Neurosci. *49*, 328–338.

Guerra, M.T., Fonseca, E.A., Melo, F.M., Andrade, V.A., Aguiar, C.J., Andrade, L.M., Pinheiro, A.C., Casteluber, M.C., Resende, R.R., Pinto, M.C., et al. (2011). Mitochondrial calcium regulates rat liver regeneration through the modulation of apoptosis. Hepatology *54*, 296–306.

Guimaraes, E., Machado, R., Fonseca, M.C., Franca, A., Carvalho, C., Araujo, E.S.A.C., Almeida, B., Cassini, P., Hissa, B., Drumond, L., et al. (2017). Inositol 1, 4, 5-trisphosphate-dependent nuclear calcium signals regulate angiogenesis and cell motility in triple negative breast cancer. PloS One *12*, e0175041.

Guzman, J.N., Sanchez-Padilla, J., Wokosin, D., Kondapalli, J., Ilijic, E., Schumacker, P.T., and Surmeier, D.J. (2010). Oxidant stress evoked by pacemaking in dopaminergic neurons is attenuated by DJ-1. Nature *468*, 696–700.

Hainaut, K., and Desmedt, J.E. (1974). Effect of dantrolene sodium on calcium movements in single muscle fibres. Nature *252*, 728–730.

Hand, K.V., Bruen, C.M., O'Halloran, F., Panwar, H., Calderwood, D., Giblin, L., and Green, B.D. (2013). Examining acute and chronic effects of short- and long-chain fatty acids on peptide YY (PYY) gene expression, cellular storage and secretion in STC-1 cells. Eur. J. Nutr. *52*, 1303–1313.

Hand, K.V., Giblin, L., and Green, B.D. (2012). Hormone profiling in a novel enteroendocrine cell line pGIP/neo: STC-1. Metab. Clin. Exp. *61*, 1683–1686.

Hawkes, C.H., Del Tredici, K., and Braak, H. (2010). A timeline for Parkinson's disease. Parkinsonism Relat. Disord. *16*, 79–84.

Hedskog, L., Pinho, C.M., Filadi, R., Ronnback, A., Hertwig, L., Wiehager, B., Larssen, P., Gellhaar, S., Sandebring, A., Westerlund, M., et al. (2013). Modulation of the endoplasmic reticulum-mitochondria interface in Alzheimer's disease and related models. Proc. Natl. Acad. Sci. U S A *110*, 7916–7921.

Heintz-Buschart, A., Pandey, U., Wicke, T., Sixel-Doring, F., Janzen, A., Sittig-Wiegand, E., Trenkwalder, C., Oertel, W.H., Mollenhauer, B., and Wilmes, P. (2018). The nasal and gut microbiome in Parkinson's disease and idiopathic rapid eye movement sleep behavior disorder. Movement Disord. *33*, 88–98.

Hijaz, B.A., and Volpicelli-Daley, L.A. (2020). Initiation and propagation of alpha-synuclein aggregation in the nervous system. Mol. Neurodegener. *15*, 19.

Hill-Burns, E.M., Debelius, J.W., Morton, J.T., Wissemann, W.T., Lewis, M.R., Wallen, Z.D., Peddada, S.D., Factor, S.A., Molho, E., Zabetian, C.P., et al. (2017). Parkinson's disease and Parkinson's disease medications have distinct signatures of the gut microbiome. Movement Disord. *32*, 739–749.

Hill, B.G., Benavides, G.A., Lancaster, J.R., Jr., Ballinger, S., Dell'Italia, L., Jianhua, Z., and Darley-Usmar, V.M. (2012). Integration of cellular bioenergetics with mitochondrial quality control and autophagy. Biol. Chem. *393*, 1485–1512.

Huo, Y., Lu, X., Wang, X., Wang, X., Chen, L., Guo, H., Zhang, M., and Li, Y. (2020). Bifidobacterium animalis subsp. lactis A6 alleviates obesity associated with promoting mitochondrial biogenesis and function of adipose tissue in mice. Molecules *25*, 1490.

Jacotot, E., Ferri, K.F., and Kroemer, G. (2000a). Apoptosis and cell cycle: distinct checkpoints with overlapping upstream control. Pathol. Biol. *48*, 271–279.

Jacotot, E., Ravagnan, L., Loeffler, M., Ferri, K.F., Vieira, H.L., Zamzami, N., Costantini, P., Druillennec, S., Hoebeke, J., Briand, J.P., et al. (2000b). The HIV-1 viral protein R induces apoptosis via a direct effect on the mitochondrial permeability transition pore. J. Exp. Med. *191*, 33–46.

Jadiya, P., Kolmetzky, D.W., Tomar, D., Di Meco, A., Lombardi, A.A., Lambert, J.P., Luongo, T.S., Ludtmann, M.H., Pratico, D., and Elrod, J.W. (2019). Impaired mitochondrial calcium efflux contributes to disease progression in models of Alzheimer's disease. Nat. Commun. *10*, 3885.

Jandu, N., Ceponis, P.J., Kato, S., Riff, J.D., McKay, D.M., and Sherman, P.M. (2006). Conditioned medium from enterohemorrhagic Escherichia coli-infected T84 cells inhibits signal transducer and activator of transcription 1 activation by gamma interferon. Infect. Immun. *74*, 1809–1818.

Jost, W.H. (2010). Gastrointestinal dysfunction in Parkinson's disease. J. Neurol. Sci. *289*, 69–73.

Kandimalla, R., Manczak, M., Yin, X., Wang, R., and Reddy, P.H. (2018). Hippocampal phosphorylated tau induced cognitive decline, dendritic spine loss and mitochondrial abnormalities in a mouse model of Alzheimer's disease. Hum. Mol. Genet. *27*, 30–40.

Karampetsou, M., Ardah, M.T., Semitekolou, M., Polissidis, A., Samiotaki, M., Kalomoiri, M., Majbour, N., Xanthou, G., El-Agnaf, O.M.A., and Vekrellis, K. (2017). Phosphorylated exogenous alpha-synuclein fibrils exacerbate pathology and induce neuronal dysfunction in mice. Scientific Rep. *7*, 16533.

Keshavarzian, A., Green, S.J., Engen, P.A., Voigt, R.M., Naqib, A., Forsyth, C.B., Mutlu, E., and Shannon, K.M. (2015). Colonic bacterial composition in Parkinson's disease. Movement Disord. *30*, 1351–1360.

Kim, S., Kwon, S.H., Kam, T.I., Panicker, N., Karuppagounder, S.S., Lee, S., Lee, J.H., Kim, W.R., Kook, M., Foss, C.A., et al. (2019). Transneuronal propagation of pathologic alpha-synuclein from the gut to the brain models Parkinson's disease. Neuron *103*, 627–641.e627.

Klingelhoefer, L., and Reichmann, H. (2015). Pathogenesis of Parkinson disease–the gut-brain axis and environmental factors. Nat. Rev. Neurol. *11*, 625–636.

Li, W., Wu, X., Hu, X., Wang, T., Liang, S., Duan, Y., Jin, F., and Qin, B. (2017). Structural changes of gut microbiota in Parkinson's disease and its correlation with clinical features. Sci. China Life Sci. *60*, 1223–1233.

Liddle, R.A. (2018). Parkinson's disease from the gut. Brain Res. *1693*, 201–206.

Lin, C.H., Chen, C.C., Chiang, H.L., Liou, J.M., Chang, C.M., Lu, T.P., Chuang, E.Y., Tai, Y.C., Cheng, C., Lin, H.Y., et al. (2019). Altered gut microbiota and inflammatory cytokine responses in patients with Parkinson's disease. J. Neuroinflammation *16*, 129.

Liu, Y., and Zhu, X. (2017). Endoplasmic reticulum-mitochondria tethering in neurodegenerative diseases. Transl. Neurodegener. *6*, 21.

Ludtmann, M.H.R., and Abramov, A.Y. (2018). Mitochondrial calcium imbalance in Parkinson's disease. Neurosci. Lett. *663*, 86–90.

Luongo, T.S., Lambert, J.P., Gross, P., Nwokedi, M., Lombardi, A.A., Shanmughapriya, S., Carpenter, A.C., Kolmetzky, D., Gao, E., van Berlo, J.H., et al. (2017). The mitochondrial Na(+)/Ca(2+) exchanger is essential for Ca(2+) homeostasis and viability. Nature *545*, 93–97.

Macpherson, A.J., Gatto, D., Sainsbury, E., Harriman, G.R., Hengartner, H., and Zinkernagel, R.M. (2000). A primitive T cell-

independent mechanism of intestinal mucosal IgA responses to commensal bacteria. Science *288*, 2222–2226.

Macpherson, A.J., and Harris, N.L. (2004). Interactions between commensal intestinal bacteria and the immune system. Nat. Rev. Immunol. *4*, 478–485.

Martinez-Martin, P., Rodriguez-Blazquez, C., Kurtis, M.M., Chaudhuri, K.R., and Group, N.V. (2011). The impact of non-motor symptoms on health-related quality of life of patients with Parkinson's disease. Movement Disord. *26*, 399–406.

McCarthy, T., Green, B.D., Calderwood, D., Gillespie, A., Cryan, J.F., and Giblin, L. (2015). STC-1 cells. In The Impact of Food Bioactives on Health: in vitro and ex vivo models, K. Verhoeckx, P. Cotter, I. Lopez-Exposito, C. Kleiveland, T. Lea, A. Mackie, T. Requena, D. Swiatecka, and H. Wichers, eds., pp. 211–220.

Mertsalmi, T.H., Aho, V.T.E., Pereira, P.A.B., Paulin, L., Pekkonen, E., Auvinen, P., and Scheperjans, F. (2017). More than constipation - bowel symptoms in Parkinson's disease and their connection to gut microbiota. Eur. J. Neurol. *24*, 1375–1383.

Morgan, K.G., and Bryant, S.H. (1977). The mechanism of action of dantrolene sodium. J. Pharmacol. Exp. Ther. *201*, 138–147.

Mun, J.K., Youn, J., Cho, J.W., Oh, E.S., Kim, J.S., Park, S., Jang, W., Park, J.S., Koh, S.B., Lee, J.H., et al. (2016). Weight change is a characteristic non-motor symptom in drug-naive Parkinson's disease patients with non-tremor dominant subtype: a Nation-wide observational study. PloS One *11*, e0162254.

Musgrove, R.E., Helwig, M., Bae, E.J., Aboutalebi, H., Lee, S.J., Ulusoy, A., and Di Monte, D.A. (2019). Oxidative stress in vagal neurons promotes parkinsonian pathology and intercellular alpha-synuclein transfer. J. Clin. Invest. *129*, 3738–3753.

Naito, Y., Uchiyama, K., and Takagi, T. (2018). A next-generation beneficial microbe: *Akkermansia muciniphila*. J Clin Biochem Nutr *63*, 33–35. https://doi.org/10.3164/jcbn.18-57.

Nalls, M.A., Saad, M., Noyce, A.J., Keller, M.F., Schrag, A., Bestwick, J.P., Traynor, B.J., Gibbs, J.R., Hernandez, D.G., Cookson, M.R., et al. (2014). Genetic comorbidities in Parkinson's disease. Hum. Mol. Genet. *23*, 831–841.

Nardelli, J., Thiesson, D., Fujiwara, Y., Tsai, F.Y., and Orkin, S.H. (1999). Expression and genetic interaction of transcription factors GATA-2 and GATA-3 during development of the mouse central nervous system. Dev. Biol. *210*, 305–321.

Nath, S., Goodwin, J., Engelborghs, Y., and Pountney, D.L. (2011). Raised calcium promotes alpha-synuclein aggregate formation. Mol. Cell. Neurosci. *46*, 516–526.

Nishiwaki, H., Ito, M., Ishida, T., Hamaguchi, T., Maeda, T., Kashihara, K., Tsuboi, Y., Ueyama, J., Shimamura, T., Mori, H., et al. (2020). Meta-analysis of gut dysbiosis in Parkinson's disease. Movement Disord. *35*, 1626–1635.

Ouwerkerk, J.P., van der Ark, K.C.H., Davids, M., Claassens, N.J., Finestra, T.R., de Vos, W.M., and Belzer, C. (2016). Adaptation of Akkermansia muciniphila to the Oxic-anoxic interface of the mucus layer. Appl. Environ. Microbiol. *82*, 6983–6993.

Perfeito, R., Lazaro, D.F., Outeiro, T.F., and Rego, A.C. (2014). Linking alpha-synuclein phosphorylation to reactive oxygen species formation and mitochondrial dysfunction in SH-SY5Y cells. Mol. Cell. Neurosci. *62*, 51–59.

Pisa, M. (1988). Regional specialization of motor functions in the rat striatum: implications for the treatment of parkinsonism. Prog. NeuroPsychopharmacol. Biol. Psychiatry *12*, 217–224.

Plovier, H., Everard, A., Druart, C., Depommier, C., Van Hul, M., Geurts, L., Chilloux, J., Ottman, N., Duparc, T., Lichtenstein, L., et al. (2017). A purified membrane protein from Akkermansia muciniphila or the pasteurized bacterium improves metabolism in obese and diabetic mice. Nat. Med. *23*, 107–113.

Prado, V.F., Martins-Silva, C., de Castro, B.M., Lima, R.F., Barros, D.M., Amaral, E., Ramsey, A.J., Sotnikova, T.D., Ramirez, M.R., Kim, H.G., et al. (2006). Mice deficient for the vesicular acetylcholine transporter are myasthenic and have deficits in object and social recognition. Neuron *51*, 601–612.

Pratico, D., Uryu, K., Leight, S., Trojanoswki, J.Q., and Lee, V.M. (2001). Increased lipid peroxidation precedes amyloid plaque formation in an animal model of Alzheimer amyloidosis. J. Neurosci. *21*, 4183–4187.

Qi, H., Li, X., Jin, Z., Simmen, T., and Shuai, J. (2020). The oscillation amplitude, not the frequency of cytosolic calcium, regulates apoptosis induction. iScience *23*, 101671.

Rani, L., and Mondal, A.C. (2020). Emerging concepts of mitochondrial dysfunction in Parkinson's disease progression: pathogenic and therapeutic implications. Mitochondrion *50*, 25–34.

Rappsilber, J., Mann, M., and Ishihama, Y. (2007). Protocol for micro-purification, enrichment, pre-fractionation and storage of peptides for proteomics using StageTips. Nat. Protoc. *2*, 1896–1906.

Reynolds, I.J., and Hastings, T.G. (1995). Glutamate induces the production of reactive oxygen species in cultured forebrain neurons following NMDA receptor activation. J. Neurosci. *15*, 3318–3327.

Sampson, T.R., Debelius, J.W., Thron, T., Janssen, S., Shastri, G.G., Ilhan, Z.E., Challis, C., Schretter, C.E., Rocha, S., Gradinaru, V., et al. (2016). Gut microbiota regulate motor deficits and Neuroinflammation in a model of Parkinson's disease. Cell *167*, 1469–1480.e1412.

Sango, K., McDonald, M.P., Crawley, J.N., Mack, M.L., Tifft, C.J., Skop, E., Starr, C.M., Hoffmann, A., Sandhoff, K., Suzuki, K., et al. (1996). Mice lacking both subunits of lysosomal beta-hexosaminidase display gangliosidosis and mucopolysaccharidosis. Nat. Genet. *14*, 348–352.

Scheperjans, F., Aho, V., Pereira, P.A., Koskinen, K., Paulin, L., Pekkonen, E., Haapaniemi, E., Kaakkola, S., Eerola-Rautio, J., Pohja, M., et al. (2015). Gut microbiota are related to Parkinson's disease and clinical phenotype. Movement Disord. *30*, 350–358.

Scherzer, C.R., Grass, J.A., Liao, Z., Pepivani, I., Zheng, B., Eklund, A.C., Ney, P.A., Ng, J., McGoldrick, M., Mollenhauer, B., et al. (2008). GATA transcription factors directly regulate the Parkinson's disease-linked gene alpha-synuclein. Proc. Natl. Acad. Sci. U S A *105*, 10907–10912.

Schneeberger, M., Everard, A., Gomez-Valades, A.G., Matamoros, S., Ramirez, S., Delzenne, N.M., Gomis, R., Claret, M., and Cani, P.D. (2015). Akkermansia muciniphila inversely correlates with the onset of inflammation, altered adipose tissue metabolism and metabolic disorders during obesity in mice. Scientific Rep. *5*, 16643.

Schneider, C.A., Rasband, W.S., and Eliceiri, K.W. (2012). NIH Image to ImageJ: 25 years of image analysis. Nat. Methods *9*, 671–675.

Scudamore, O., and Ciossek, T. (2018). Increased oxidative stress exacerbates alpha-synuclein aggregation in vivo. J. Neuropathol. Exp. Neurol. *77*, 443–453.

Shevchenko, A., Wilm, M., Vorm, O., and Mann, M. (1996). Mass spectrometric sequencing of proteins silver-stained polyacrylamide gels. Anal. Chem. *68*, 850–858.

Smedler, E., and Uhlen, P. (2014). Frequency decoding of calcium oscillations. Biochim. Biophys. Acta *1840*, 964–969.

Sovran, B., Hugenholtz, F., Elderman, M., Van Beek, A.A., Graversen, K., Huijskes, M., Boekschoten, M.V., Savelkoul, H.F.J., De Vos, P., Dekker, J., et al. (2019). Age-associated impairment of the mucus barrier function is associated with profound changes in microbiota and immunity. Scientific Rep. *9*, 1437.

Spillantini, M.G., Schmidt, M.L., Lee, V.M., Trojanowski, J.Q., Jakes, R., and Goedert, M. (1997). Alpha-synuclein in Lewy bodies. Nature *388*, 839–840.

Stefanis, L. (2012). alpha-Synuclein in Parkinson's disease. Cold Spring Harb. Perspect. Med. *2*, a009399.

Surmeier, D.J., and Schumacker, P.T. (2013). Calcium, bioenergetics, and neuronal vulnerability in Parkinson's disease. J. Biol. Chem. *288*, 10736–10741.

Tenreiro, S., Eckermann, K., and Outeiro, T.F. (2014). Protein phosphorylation in neurodegeneration: friend or foe? Front. Mol. Neurosci. *7*, 42.

Tinel, H., Cancela, J.M., Mogami, H., Gerasimenko, J.V., Gerasimenko, O.V., Tepikin, A.V., and Petersen, O.H. (1999). Active mitochondria surrounding the pancreatic acinar granule region prevent spreading of inositol trisphosphate-evoked local cytosolic Ca(2+) signals. EMBO J. *18*, 4999–5008.

Tjalsma, H., Bolhuis, A., Jongbloed, J.D., Bron, S., and van Dijl, J.M. (2000). Signal peptide-dependent protein transport in Bacillus subtilis: a genome-based survey of the secretome. Microbiol. Mol. Biol. Rev. *64*, 515–547.

Tompa, P., Toth-Boconadi, R., and Friedrich, P. (2001). Frequency decoding of fast calcium oscillations by calpain. Cell Calcium *29*, 161–170.

Tsarovina, K., Pattyn, A., Stubbusch, J., Muller, F., van der Wees, J., Schneider, C., Brunet, J.F., and Rohrer, H. (2004). Essential role of Gata transcription factors in sympathetic neuron development. Development *131*, 4775–4786.

Unger, M.M., Spiegel, J., Dillmann, K.U., Grundmann, D., Philippeit, H., Burmann, J., Fassbender, K., Schwiertz, A., and Schafer, K.H. (2016). Short chain fatty acids and gut microbiota differ between patients with Parkinson's disease and age-matched controls. Parkinsonism Relat. Disord. *32*, 66–72.

Vidal-Martinez, G., Chin, B., Camarillo, C., Herrera, G.V., Yang, B., Sarosiek, I., and Perez, R.G. (2020). A pilot microbiota study in Parkinson's disease patients versus control subjects, and effects of FTY720 and FTY720-mitoxy therapies in parkinsonian and multiple system Atrophy mouse models. J. Parkinson's Dis. *10*, 185–192.

Vos, M., Lauwers, E., and Verstreken, P. (2010). Synaptic mitochondria in synaptic transmission and organization of vesicle pools in health and disease. Front. Synaptic Neurosci. *2*, 139.

Wakabayashi, K., Mori, F., Tanji, K., Orimo, S., and Takahashi, H. (2010). Involvement of the peripheral nervous system in synucleinopathies, tauopathies and other neurodegenerative proteinopathies of the brain. Acta Neuropathol. *120*, 1–12.

Wang, Y., Prpic, V., Green, G.M., Reeve, J.R., Jr., and Liddle, R.A. (2002). Luminal CCK-releasing factor stimulates CCK release from human intestinal endocrine and STC-1 cells. Am. J. Physiol. Gastrointest. Liver Physiol. *282*, G16–G22.

Williams, G.S., Boyman, L., Chikando, A.C., Khairallah, R.J., and Lederer, W.J. (2013). Mitochondrial calcium uptake. Proc. Natl. Acad. Sci. U S A *110*, 10479–10486.

Zaichick, S.V., McGrath, K.M., and Caraveo, G. (2017). The role of Ca(2+) signaling in Parkinson's disease. Dis. Model Mech. *10*, 519–535.

Zhao, F., Li, P., Chen, S.R., Louis, C.F., and Fruen, B.R. (2001). Dantrolene inhibition of ryanodine receptor Ca2+ release channels. Molecular mechanism and isoform selectivity. J. Biol. Chem. *276*, 13810–13816.

Zhao, S., Liu, W., Wang, J., Shi, J., Sun, Y., Wang, W., Ning, G., Liu, R., and Hong, J. (2017). Akkermansia muciniphila improves metabolic profiles by reducing inflammation in chow diet-fed mice. J. Mol. Endocrinol. *58*, 1–14.

STAR★METHODS

KEY RESOURCES TABLE

REAGENT or RESOURCE	SOURCE	IDENTIFIER
Antibodies		
α-Synuclein (αSyn)	Abcam	(Cat# ab51252, RRID:AB_869971)
pSer129 α-Synuclein (Rabbit monoclonal)	Abcam	(Cat# 2014-1, RRID:AB_765074
anti-GATA2 (Mouse polyclonal)	R and D systems	Cat# MAB2046, RRID:AB_2108424)
anti-β-actin (Mouse monoclonal)	Santa Cruz Biotechnology	Cat# sc-47778 HRP, RRID:AB_2714189
anti-aggregated αSyn	Abcam	(Cat# ab209538, RRID: AB_2714215
Bacterial and virus strains		
Akkermansia muciniphila	DSMZ	DSM 22959, Type strain
E.coli	ATCC	ATCC 25922
Biological samples		
Human fetal brain cDNA library	Clontech	Cat# HL3003a
Chemicals, peptides, and recombinant proteins		
Fluo-4/AM	Thermo-Fisher	F14201; CAS#: 273221-67-3
Rhod-2/AM	Thermo-Fisher	R1245M; CAS#: 145037-81-6
Dihydroethidium (Hydroethidine)	Thermo-Fisher	D11347; CAS# 38483-26-0
Mucin from porcine stomach	Sigma-Aldrich	M2378; CAS#: 84082-64-4
Thapsigargin	Sigma-Aldrich	240117; CAS: 629-11-8
FuGene HD	Promega	E2311
Dantrolene Sodium Salt	Sigma-Aldrich	D9175; CAS# 14663-23-1
MitoTracker Red CMXROS	Thermo-Fisher	M7512; CAS#: 167095-09-2
Critical commercial assays		
Cholecystokinin EIA Kit	Sigma-Aldrich	RAB0039
CellTiter 96® AQueous One Solution Cell Proliferation Assay (MTS)	Promega	G3582
Experimental models: Cell lines		
STC-1	ATCC	(Cat# CRL-3254, RRID:CVCL_J405)
Experimental models: Organisms/strains		
FVB *Mus musculus*	The Jackson Laboratory	N/A
Oligonucleotides		
Primer: HsSnca.M1 forward: 5′- CATCTAAGC TTGCCATGGATGTATTCATGAAAGGAC -3′; reverse: 5′-ATGACACCCGGGGGCTTCAGG TTCGTAGTCTTGATAC -3′;	This paper	N/A
Primer: *Akkermansia muciniphila* AM1: 5′- CAGCACGTGAAGGTGGGGAC -3′; AM2: 5′- CCTTGCGGTTGGCTTCAGAT -3′	(Collado et al., 2007)	N/A
Recombinant DNA		
Plasmid: pAc1GFP1-Parvalbumin-GFP	(Guerra et al., 2011)	6084-1
Plasmid: pAc1GFP1-Parvalbumin-Mito-GFP	(Guerra et al., 2011)	632524
Plasmid: pcDNA5mCherry-hαSyn	This paper	N/A
Plasmid: pEGFP-hαSyn	This paper	N/A

(*Continued on next page*)

Continued

REAGENT or RESOURCE	SOURCE	IDENTIFIER
Plasmid: pEGFP-C1	Addgene	6084-1
Plasmid: pmCherry-C1	Addgene	632524
Software and algorithms		
Image J	(Schneider et al., 2012)	https://imagej.nih.gov/ij/
Graphpad Prism 8	GraphPad Software, Inc	https://www.graphpad.com/scientific-software/prism/
MaxQuant 1.3	Max-Planck-Institute of Biochemistry	https://www.maxquant.org/

RESOURCE AVAILABILITY

Lead contact

Further information and requests for resources and reagents should be directed to and will be fulfilled by the lead contact, Matheus de Castro Fonseca (hp.matheus@gmail.com).

Materials availability

This study did not generate new unique reagents.

Data and code availability

- All data reported in this paper will be shared by the lead contact upon request
- This paper does not report original code.
- Any additional information required to reanalyze the data reported in this paper is available from the lead contact upon request.

EXPERIMENTAL MODELS AND SUBJECT DETAILS

Cell lines

STC-1 (CRL-3254) cell line was obtained from the America Type Culture Collection (ATCC). STC-1 cell was cultured in DMEM (Gibco) supplemented with 10% fetal bovine serum (FBS), 1% penicillin/streptomycin antibiotics (PSA) and incubated at 37°C with 5% CO2: 95% air.

Lyophilized *A. muciniphila* (DSM-22959) and *E. coli* (ATCC 25922) were purchased from DSMZ and America Type Culture Collection respectively. Strains were grown individually in pure Brain & Heart Infusion Broth (BHI) (BD, Heidelberg, Germany) or in BHI broth supplemented with 0.4% mucin (Sigma-Aldrich, MO, USA) (Derrien et al., 2004; Huo et al., 2020; Zhao et al., 2017)

Animals

Young (4-months) and old (18–20 months) SPF male FVB mice were maintained under specific pathogen-free conditions. After 1–2 weeks of acclimation, old mice were randomly assigned to two groups. Group AKK (*A. muciniphila*) mice were administrated $2*10^8$ *A. muciniphila* cells determined by OD 600nm (Ouwerkerk et al., 2016) suspended in 0.15 mL sterile anaerobic PBS by oral gavage per day, while mice in Group Control (PBS) were given an equivalent volume of sterile anaerobic PBS instead (Plovier et al., 2017). Treatment was continued for 28 days. All mice were maintained in a temperature- and humidity-controlled environment under a 12-h light–dark cycle and had *ad libitum* access to food and water. All experiments were approved by the Institutional Committee of Animal Use & Protection (CEUA 92-B).

METHOD DETAILS

Fecal microbial community analysis

To confirm the effectiveness of *A. muciniphila* oral administration, fecal samples were collected before and after the last day of treatment, immediately frozen and stored at −80°C freezer after collection. Total bacterial DNA was extracted from fecal samples (approximately 200 mg) using a QIAamp FastDNA Stool Mini Kit (Qiagen, Hilden, Germany) following the manufacturer's procedures. Specific primers for detection of the variable regions of the 16S rRNA gene sequence of *A. muciniphila* were used (AM forward-CAGCACGTGAAGGTGGGGAC; AM reverse CCTTGCGGTTGGCTTCAGAT) (Collado et al., 2007). All

reactions were carried out on an Applied Biosystems® 7900HT Fast Real-Time PCR machine (Applied Biosystems® Foster City, CA, USA). Each reaction was performed in duplicate and consisted of 1X Syber®Green PCR Master Mix (Applied Biosystems), forward and reverse primers at final concentration of 200 nM and 4 μL of template. Standard cycling conditions and melt curve analysis were employed. The cycle threshold (CT) value of each sample was then compared with a standard curve made by diluting genomic DNA of *A. muciniphila*. Log10 of *A. muciniphila* number per gram of fecal content was used to indicate the abundance of *A. muciniphila* (Grander et al., 2018)

Quantification of fecal mucin

Mucin was extracted from each 100 mg fecal sample. Fecal mucin contents were determined using a fecal mucin assay kit (Mucin Assay Kit, Cosmo Bio, Co., Ltd., Tokyo, Japan). A fluorometric assay discriminated O-linked glycoproteins (mucins) from N-linked glycoproteins. Fluorescence was measured using a SoftMax®Pro spectrometer (Molecular Devices, CA, USA).

Behavioral tests

To determine the possible effects of *A.muciniphila* of sensory motor function in mice, wire-hang, cylinder and beam walking test were performed. To acclimatize to the behavioral testing condition, the mice were trained on the last 2 days before the last gavage. Tests were performed as per the protocol described with slight modification (Fleming et al., 2013). For the cylinder test, a transparent glass cylinder with a 14-cm diameter and 19-cm height was used. A video recording device was set up and mice were then placed inside the cylinder one-by-one for a 3-min recording period to estimate the number of rearing. The number of rearing was defined as the number of times the mouse stood with the support of its hind limbs solely. Thorough cleaning of the cylinder was performed between experiments. The wire-hang test is a useful tool to evaluate motor function and motor strength in rodents, and the experiments were performed according to Sango et al. (1996) and Prado et al. (2006) (Prado et al., 2006; Sango et al., 1996).We placed each animal individually in the top of a wire cage lid (22 × 22 cm) and then the lid was gently turned upside down by the investigator. The latency of mice to lose their grip and fall off the lid was visually evaluated in three trials with a cut-off time of 60s. Beam walking test was performed to access the motor coordination requiring balance and equilibrium. Animals were made to train to walk on a stationary wooden narrow flat beam (L100cm×W1cm) placed at a height of 100 cm from the floor. Time to walk the beam from one end to the other was counted as described (Pisa, 1988). Mice were habituated at the behavioral room 2 h before the tests.

Conditioned media collection

Briefly, lyophilized *A. muciniphila* (DSM-22959) and *E. coli* (ATCC 25922) were grown individually in pure Brain & Heart Infusion Broth (BHI) (BD, Heidelberg, Germany) or in BHI broth supplemented with 0.4% mucin (Sigma-Aldrich, MO, USA) (Derrien et al., 2004; Huo et al., 2020; Zhao et al., 2017).After being supplemented and sterilized, the vials containing the media were gassed with N_2 injection system for 30 minutes, and then placed into an anaerobic chamber (Whitley DG250 Anaeorobic Workstation, Don Whitley Scientific) kindly provided by the Brazilian Bio renewables National Laboratory (LNBR, CNPEM). The bacterial inoculum was incubated for up to 72 hs at 37°C. After 12, 24, 36, 48, 60 and 72 hs of incubation, an aliquot of each of the vials was collected and evaluated under light microscopy and spectrometry for optical density (OD) measurement, using a spectrometer (Evolution™ 60S UV-Visible Spectrophotometer, Thermo Fisher Scientific Inc.) in order to monitor bacterial growth.

After 36-40 hs of incubation, conditioned (CM) and unconditioned media were collected and concentrated. Briefly, media were centrifuged for 4000 rpm at 4°C to pellet cells and the supernatant was concentrated at 4000 rpm at 4°C for 20min using Centricon® 3kD Plus-70 Centrifugal Filter Units to separate the protein fraction from small molecules and other metabolites. These conditioned (BHI CM) or unconditioned media (BHI) containing were then filtered (0.22 μm) and stored at −80°C until used. For some experiments, conditioned media as heat inactivated by boiling (100 °C, 2 hs) (Jandu et al., 2006).Subsequently, conditioned medium was cooled to 37 °C and employed in calcium signaling experiments.

Mass spectrometry

A. muciniphila CM and CM + 0.4% mucin were submitted to protein electrophoresis technique using 10% acrylamide-SDS page separation. After the electrophoretic run, the lanes were cut into small fragments,

micro-purified, enriched, and digested using trypsin (Rappsilber et al., 2007; Shevchenko et al., 1996). Then, samples were directed to mass spectrometry (LTQ Orbitrap Velos, Thermo-Fischer). The peptides were separated with a 2–30% acetonitrile gradient in 0.1% formic acid using a PicoFrit analytical column (20 cm × 75 nm, particle size from 5 μm, New Objective) at a flow rate of 300 nL/min over 173 min. The nano-electrospray voltage was adjusted to 2.2 kV and the source temperature was set at 275 °C. All instrument methods were set in data dependent acquisition mode. The full scan MS spectra (m/z300-1600) were acquired in the Orbitrap analyzer after accumulation to a target value of 1x106. The resolution in the Orbitrap was set at 60,000 and the 20 ions of the most intense peptides with states of charge $\geq$2 were sequentially isolated to a target value of 5,000 and fragmented into linear ion traps using low energy CID (35% normalized collision energy). The signal limit for triggering the MS/MS event was set to 1,000 counts. Dynamic exclusion was activated with an exclusion size list of 500, exclusion duration of 60 s and a repeat count of 1. An activation q = 0.25 and an activation time of 10 ms were used.

The data obtained by mass spectrometry were processed using the MaxQuant 1.3 software based on the *A. muciniphila* protein database.

^{1}H NMR spectra acquisition

For NMR acquisitions, 540 μL of each conditioned media before and after centrifugation with Centricon® 3kD Plus-70 Centrifugal Filter Units were mixed with 60 μL of phosphate buffer (1 M, pH 7.4) containing 5 mM of TMSP-d4 [Sigma-Aldrich 3- (trimethylsilyl) −2,2 ′, 3,3′-tetradeuteropropionic acid; as reference or internal standard] to produce a final 600 μL solution, then transferred to a 5 mm NMR tube (Norell Standard Series 5 mm, Sigma-Aldrich) for immediate acquisition.

The ^{1}H NMR spectra of the samples were acquired using an Agilent Inova 500 spectrometer (Agilent Technologies Inc.™, Santa Clara, EUA) from Brazilian Biosciences National Laboratory (Brazilian Center for Research in Energy and Materials - CNPEM) equipped with a triple resonance cryoprobe and operating at a Larmor frequency of 599.887 MHz and constant temperature of 298 K (25°C). A total of 256 or 1024 free induction decays, depending on the concentration of metabolites, were collected with 32 k data points over a spectral width of 16 ppm and acquisition time of 4s. A 1.5 s relaxation delay was incorporated between scans, during which a continual water pre-saturation radio frequency (RF) field was applied to eliminate residual water signal. The software used for the acquisition and processing of FIDs was Agilent's VnmrJ.

Assignment and quantification of the metabolites

The metabolites were processed and quantified using NMR Suite software version 8.1 (Chenomx Inc™, Edmonton, AB, Canada). Processor module of this software was used to adjust the spectral phase and baseline corrections. A 0.5 Hz line-broadening function was used to reduce signal noise and facilitate the fitting of the metabolite signals in spectral peaks. The water signal was suppressed, and the spectra were calibrated using the reference signal of the TMSP-d4 as 0.5 mM. The spectra were individually transferred to the Profiling module of this software to determine the acetate and propionate levels of each group. Metabolites were identified and their concentrations were measured. Metabolite concentration data were exported to Excel® (Microsoft Office™ 365) and normalized, when necessary.

Plasmids and transfection

cDNA for the Ca^{2+} binding protein parvalbumin (PV) fused to mitochondrial targeting sequence (PV-MTS-GFP) and respective control (MTS-GFP) were kindly donated by Dr. Mateus Guerra (Yale University, USA (Guerra et al., 2011). cDNA for the human αSyn (αSyn) was amplified and cloned between the HindIII and SmaI restriction sites of pEGFP-N2 vector. For αSyn mCherry-tagged version, the human αSyn sequence was inserted between BamH1 and SalI of the pCDNA5-mCherry vector. Cells were transfected with FUGENE HD (Promega) accordingly to manufacturer's instruction.

Immunofluorescence

Cells were cultured onto glass-slides and fixed with 4% PFA for 20 min. Samples were blocked in PBS 1X containing 5% Normal Horse Serum and 5% bovine albumin (Sigma-Aldrich) for 1h. After washing in PBS 1X, cells were incubated with primary antibodies anti-αSyn (1:250, Abcam); anti-pser129 αSyn, (1:100; Abcam) for 2 h at room temperature, followed by PBS washes and incubation with secondary

antibody (anti-mouse Alexa-488, 1:500; Thermo-Fischer) for 1 h at room temperature. Fluorescence intensity of αSyn and αSyn-p-serine-129 was quantified on at least 25 cells from 3 different experiments. Data are expressed as percentage relative to the untreated group (control). The images were obtained using a Leica SP8 confocal microscope, using a ×63 objective lens, 1.4 NA.

Total RNA was extracted using TRIzol Reagent (Life Technologies, Grand Island, NY) and cDNA generated with ThermoScript (Invitrogen). real-time PCR analysis based upon the intercalation of SYBR® Green on an ABI prism 7900 HT Fast Real Time PCR system (PE Applied Biosystems). The expression level of each gene was normalized to GAPDH. Samples were analyzed in triplicate from 5 different mouse ileum specimens.

Cell viability

Cellular viability was measured using the CellTiter 96® AQueous One Solution Cell Proliferation Assay (MTS) (Promega) according to the manufacturer's protocol. STC-1 cells were treated with 1 or 10% BHI and BHI CM for 48 hs. Following this period, cells were incubated in the presence of MTS Tetrazolium Compound for 2 hr at 37°C. Absorbance measurements (490nm) were performed using a plate reader (PerkinElmer; Waltham, MA).

Immunoblotting

Cell proteins were extracted with RIPA buffer supplemented with inhibitors of proteases and phosphatases followed by centrifugation at 10,000 rpm for 10 min at 4º C. Proteins were separated by SDS-PAGE in 12% Bis-Tris gels and transferred onto 0.45 μm nitrocellulose membranes (BioRad). For dot blot quantification of aSyn fibrils, 1 μg of tissue homogenate from the specified region was spotted in 1 μL volume aliquots onto 0.45 mm nitrocellulose membranes. The blots were incubated overnight at 4°C with anti-αSyn (1:1000, Abcam), GATA-2 (1:1000, R and D Systems), anti-pser129 αSyn, (1:1000; Abcam) and anti-aggregated αSyn (1:2000, Abcam) antibodies followed by incubation with horseradish peroxidase (HRP)-conjugated secondary IgGs (anti-rabbit, 1:5000, Thermo-Fischer; anti-mouse, 1:5000, Thermo Fischer). β-actin (1:5000, Santa Cruz) or GAPDH (1:5000, Santa Cruz) were used as loading controls. Membranes were developed using the BioRad chemiluminescence detection system (Clarity Western ECL, BioRad). Chemiluminescence signals were quantified using Image J software. β -actin or GAPDH was used as a loading control.

Cytosolic and mitochondrial calcium measurements

For cytosolic calcium measurements, cells were loaded with the Ca^{2+} indicator Fluo-4/AM (for intracellular Ca^{2+}) or Rhod-2/AM (for mitochondrial Ca^{2+}) (Thermo Fisher Scientific) for 15 min at 37°C, placed onto the stage of a Leica SP8 Confocal System and continuously perfused with HEPES buffer solution (142.2 mM NaCl, 5.4 mM KCl, 1.0 mM NaH_2PO_4, 10 mM HEPES, 5.6 mM dextrose, 0.8 mM MgSO4 and 1 mM $CaCl_2$), unless otherwise noted. 1 or 10% BHI or BHI CM (v/v) medium with or without 0.4% mucin was used to trigger Ca^{2+} release. 40 μM Adenosine triphosphate (ATP) was used to trigger InsP3-dependent Ca^{2+} release and to evaluate mitochondrial-calcium response after 48h-treatment with the conditioned medium. To investigate whether intracellular calcium signaling was from endoplasmic reticulum stores, cells were incubated for 30 min in HEPES Ca^{2+}-free buffer containing 10μM thapsigargin prior to stimulation with the conditioned medium. To investigate IP3 dependence for the *A. muciniphila* conditioned media-triggered calcium response, cells were incubated with Fluo-4/AM and 2.5 μM xestospongin C for 30 min before stimulation with the conditioned medium. Dantrolene sodium salt (75 μM) was used as RYR blocker. For mitochondrial calcium measurements in PV-MTS-GFP or MTS-GFP transfected cells, cells were transfected 48 hs before the experiment using FUGENE HD (Promega) according to the manufacturer's instructions. Data are expressed as fluorescence/baseline fluorescence × 100% of the average values of samples from 3-6 biological replicates (>20 cells/replicate). The images were obtained using a Leica SP8 confocal microscope, using a ×63 objective lens, 1.4 NA, excitation at 488 nm and emission at 505-525 nm for both dyes.

Detection of reactive oxygen species (ROS)

To evaluate the formation of reactive oxygen species (ROS), STC-1 cells were previously seeded on glass slides were treated with 5 μM DHE (Thermo-Fischer) for 30 min in HEPES buffer solution (142.2 mM NaCl, 5.4 mM KCl, 1.0 mM NaH_2PO_4, 10 mM HEPES, 5.6 mM dextrose, 0.8 mM $MgSO_4$ and 1 mM $CaCl_2$). The glass slides were transferred to a perfusion chamber attached to the confocal microscope. The cells were

stimulated with 1 or 10% (v/v) *A. muciniphila* conditioned or unconditioned media. As a positive control of ROS formation, 100 μM H_2O_2 was used.

For each stimulus, the emission of fluorescence in response to the general indicator of oxidative stress was monitored in individualized cells during stimulation with the conditioned and unconditioned media. Data are expressed as fluorescence/baseline fluorescence × 100% of the average values of samples from 3-6 biological replicates (>20 cells/replicate). The images were obtained using a Leica SP8 confocal microscope, using a ×63 objective lens, 1.4 NA, excitation at 488–518 nm and emission at 606 nm.

Evaluation of mitochondrial membrane potential

STC-1 cells were treated for 48 hs with 1 or 10% (v/v) *A. muciniphila* conditioned or unconditioned media and then incubated 500 nM of MitoTracker Red CMXRos (Thermo-Fischer) for 30 min. Cells were washed 2x with PBS1x and then fixed in 4% paraformaldehyde at room temperature, for 20 min, washed with PBS and in sequence, were mounted in Vectashield. At least 25 cells from 3 different experiments were analyzed. Data are expressed as percentage relative to the untreated group (control). The images were obtained using a Leica SP8 confocal microscope, using a ×63 objective lens, 1.4 NA, excitation at 579 nm and emission at 599 nm. Finally, the intensity of fluorescence of the dye was quantified

Immunohistofluorescence

Mice were euthanized and perfused with 4% paraformaldehyde. Ileum was harvested, embedded in 4% low melting agarose and sections (100μm) were collected with a Vibratome VT1000S (Leica). All sections were rinsed with 1X PBS, permeabilized with 0.5% Triton X-1000 solution and blocked in 10% normal horse serum in 10 mM Tris, pH 7.4, 0.9% NaCl, 0.1% Triton X-100 (TBST) for 60 minutes at room temperature to limit nonspecific antibody association. After washing in PBS 1X, cells were incubated with primary antibodies anti-αSyn conformation specific (1:250, Abcam); and anti-CCK (1:100, Abcam) overnight at 4°C, followed by PBS washes and incubation with secondary antibody and rhodamine-phalloidin (Thermo Fisher Scientific) for 1 h at room temperature. Slices were mounted in Vectashield solution containing DAPI.

QUANTIFICATION AND STATISTICAL ANALYSIS

Data analysis for PCR assays performed on the Applied Biosystems platform was performed using SDS 2.4 software (Applied Biosystems®). Target copy number in each sample was determined based on the fold change ($2-\Delta Ct$) relative to the 107 DNA standard. Copy numbers were normalized for dilution volume, elution volume, DNA concentration and sample weight. The statistical relevance of the bar graphs was obtained by calculating the P-value using the unpaired two-tailed Student's *t-test* (*). The bar graphs showed in the Figures are presented as mean ± SEM. For the imaging experiments, at least 25 independent cells for each condition were analyzed using the software Image J (Schneider et al., 2012). Comparison of multiple groups was performed by one-way analysis of variance with Bonferroni post-tests. All column graphs, plots and statistical analyses were done using GraphPad Prism version 6 software. Detailed information regarding statistic test and number of experiments are embedded in figure legends.